Lactate Dehydrogenase B Controls Lysosome Activity and Autophagy in Cancer

Lucie Brisson, Piotr Bański, Martina Sboarina, Coralie Dethier, Pierre Danhier, Marie-Joséphine Fontenille, Vincent F van Hée, Thibaut Vazeille, Morgane Tardy, Jorge Falces, et al.

Lactate dehydrogenase B controls lysosome activity and autophagy in cancer

Lucie Brisson[1], Piotr Bański[1], Martina Sboarina[1], Coralie Dethier[1], Pierre Danhier[1,2], Marie-Joséphine Fontenille[1], Vincent F. Van Hée[1], Thibaut Vazeille[1], Morgane Tardy[1], Jorge Falces[1], Caroline Bouzin[3], Paolo E. Porporato[1], Raphaël Frédérick[2], Carine Michiels[4], Tamara Copetti[1], and Pierre Sonveaux[1,*]

---

[1]Institut de Recherche Expérimentale et Clinique (IREC), Pole of Pharmacology, Université catholique de Louvain (UCL), 1200 Brussels, Belgium

[2]Louvain Drug Research Institute (LDRI), Université catholique de Louvain (UCL), 1200 Brussels, Belgium.

[3]IREC Imaging Platform, Université catholique de Louvain (UCL), 1200 Brussels, Belgium

[4]URBC-NARILIS, University of Namur, 5000 Namur, Belgium.

T.C. and P.S. are co-last authors

[*]Correspondence: pierre.sonveaux@uclouvain.be, phone: +32 2 764 52 67, fax: +32 2 764 52 69.

Running title: LDHB controls autophagy

Abstract word count: 108/120

Significance paragraph word count: 105/120

Total character count: 59,595/60,000

SUMMARY

Metabolic adaptability is essential for tumor progression and includes cooperation between cancer cells with different metabolic phenotypes. Optimal glucose supply to glycolytic cancer cells occurs when oxidative cancer cells use lactate preferentially to glucose. However, using lactate instead of glucose mimics glucose deprivation, and glucose starvation induces autophagy. We report that lactate sustains autophagy in cancer. In cancer cells preferentially to normal cells, lactate dehydrogenase B (LDHB), catalyzing the conversion of lactate and NAD^+ to pyruvate, NADH and H^+, controls lysosomal acidification, vesicle maturation and intracellular proteolysis. LDHB activity is necessary for basal autophagy and cancer cell proliferation, not only in oxidative but also in glycolytic cancer cells.

SIGNIFICANCE

Autophagy promotes cancer cell survival and proliferation by recycling damaged proteins and organelles in case of oxidative stress and by ensuring metabolite supplementation under nutrient starvation. We identified that lactate dehydrogenase B (LDHB) controls autophagy in cancer. LDHB catalyzes the conversion of lactate and NAD^+ to pyruvate, NADH and H^+. This reaction promotes lysosomal acidification dependent on V-ATPase, a proton pump of lysosomes. Lysosomal acidification is essential for vesicle maturation and protease activation during autophagy. Consequently, lactate oxidation by LDHB promotes autophagy in oxidative and glycolytic cancer cells. Conversely, targeting LDHB activity inhibits autophagy and the proliferation of cancer cells preferentially to normal differentiated cells.

INTRODUCTION

Cancer can be viewed as a metabolic disease in which cancer cells strive to fulfill their proliferative agenda in a microenvironment characterized by uneven and fluctuating resource bioavailability. Oxygen and nutrient shortage are well-known characteristics of cancer that result from a mismatch between supply and use, inherent to blood perfusion abnormalities and high consumption rates (Walenta et al., 2001; Dewhirst et al., 2008). At least three different evolutionary metabolic strategies allow cancer cells to cope with fluctuating resource availability.

First, unlike most normal cells, cancer cells are characterized by a high metabolic plasticity allowing them to switch substrates depending on availability. While hypoxic cancer cells are addicted to glucose-fueled anaerobic glycolysis, oxidative cancer cells close to tumor-feeding blood vessels can use several precursor substrates in order to fuel oxidative phosphorylation, among which glucose, glutamine, lactate and lipids represent the main available pools (Porporato et al., 2011; Dhup et al., 2012; Hensley et al., 2013). Fine-tuning the biosynthetic/bioenergetic balance is controlled at the enzymatic level to match cell needs (Warburg, 1956; Mazurek, 2011; Mullen et al., 2012).

Upon nutrient starvation, a metabolic strategy of cancer cells is to increase autophagy (White, 2012). During the autophagic process, an autophagosome is formed that isolates targeted or non-specific material. This content then undergoes enzymatic degradation after the fusion of the autophagosome with lysosomes that provide protons and acid-activated proteases to the so formed autolysosome (Levine and Kroemer, 2008). Degradation products can then be exported or recycled (Rabinowitz and White, 2010). Either excessive or long term activation of autophagy or its inhibition with agents such as chloroquine may lead to cell death (Maclean et al., 2008; Yoon et al., 2010). Inhibition of autophagy in particular constitutes a promising therapeutic approach against cancer. Autophagy also offers cytoprotection by recycling damaged proteins and organelles when cancer cells

face redox stress (White, 2012). Additional metabolic resources can be obtained when cancer cells exploit the metabolic activities of stromal cells, such as fibroblasts, adipocytes and muscle cells (Commisso et al., 2013; Icard et al., 2014); an extreme form of which is cannibalism for nutrient and functional organelle supply (Krajcovic and Overholtzer, 2012; Tan et al., 2015).

A third metabolic strategy promoting tumor progression is cooperativeness. A good example is when oxidative cancer cells oxidatively recycle lactate provided by glycolytic cancer cells, thus sparing glucose and optimizing its biodisponibility as a glycolytic fuel for hypoxic cancer cells (Sonveaux et al., 2008; Kennedy et al., 2013). The oxidative use of lactate by oxygenated cancer cells depends on its uptake, a process facilitated by monocarboxylate transporters (MCTs, of which MCT1 is the main contributor), and on the oxidation of lactate in pyruvate by lactate dehydrogenase B (LDHB). Pyruvate then fuels the TCA cycle (Dhup et al., 2012). This pathway represses glycolysis because of a competition between LDHB and the glycolytic enzyme glyceraldehyde-3-phosphate dehydrogenase for NAD^+ and owing to an allosteric inhibition of glycolytic enzymes hexokinase and phosphofructokinase-1 by lactate (Leite et al., 2011; Dhup et al., 2012). Cooperativeness based on the preferential use of lactate compared to glucose by oxidative cancer cells was coined ‘metabolic symbiosis’ (Sonveaux et al., 2008). It is a hallmark of many cancer types (Sonveaux et al., 2008; Ho et al., 2012; Guillaumond et al., 2013; Curry et al., 2013; Kennedy et al., 2013). However, while improved glucose delivery is a net advantage for glycolytic cancer cells, its benefit for oxidative cancer cells is still elusive. This study addresses this open question.

RESULTS

LDHB controls tumor progression and cancer cell proliferation

Using oxidative SiHa human cervix adenocarcinoma cells as main model, we previously proposed that oxidative lactate metabolism is at the core of a metabolic symbiosis based on the exchange of lactate in cancer (Sonveaux et al., 2008; Dhup et al., 2012). This pathway requires MCT1-facilitated lactate uptake and lactate oxidation to pyruvate by LDHB (Halestrap and Wilson, 2012). To further evidence the significance of lactate oxidation in cancer, we retrospectively analyzed a microarray dataset of 332 uterine cancer patients. We found that high expression of *MCT1/SLC16A1* together with *LDHB* predicts poor overall patient survival (**Figure 1A**). Taken independently, *MCT1* and *LDHB* were significantly associated with poor patient prognosis, but *LDHA*, catalyzing the reduction of pyruvate to lactate in glycolytic cancer cells, was not. Clinical data thus suggested that, contrary to its closest relative LDHA, LDHB could control the clinical progression of uterine cancers. We therefore aimed to experimentally characterize the specific contribution of LDHB to tumor progression. We engineered SiHa cells expressing a TET-on shRNA targeting LDHB (shLDHB-1) or a control shRNA (shCTR) that were used to generate tumors in mice. To preserve tumor take, doxycycline was administered one day after tumor implantation. Compared to shCTR, doxycycline-induced shLDHB-1 expression caused significant yet transient tumor growth retardation (**Figure 1B**). Analysis of tumors at the end of the experiments revealed no re-expression of LDHB and no compensation of LDHB silencing by increased LDHA expression (**Figure 1C**). Silencing LDHB was associated with increased apoptosis (caspase 3 cleavage, **Figure 1D**) and decreased cell proliferation (**Figure 1E**). In vitro assays using the same system (cells were treated during 7 days with doxycycline, then an equal number of cells were plated for an additional 3 days of treatment with doxycycline) recapitulated our in vivo observations by showing early but not late decrease in SiHa cell number by

shLDHB-1, despite effective LDHB silencing (**Figure 1F**). We used the same strategy to induce a second inducible shRNA (shLDHB-2) in mice bearing a HCT116 human colon carcinoma xenograft. Doxycycline was administered 12 days after tumor implantation once tumors reached 5 mm diameter. Silencing LDHB caused significant HCT116 growth retardation (**Figure S1A-B**).

Our data indicated that, in cancers, LDHB controls early tumor progression and the number of cancer cells, and negatively impacts patient survival. To better delineate the contribution of LDHB to malignancy, we tested other cancer cell lines. Silencing LDHB with a siRNA (siLDHB-2) decreased cell number in all the cancer cell lines that we investigated: HeLa cervix cancer cells, MCF7 human breast cancer cells, HCT116 and WiDr human colon carcinoma cells, SKOV3 human ovarian carcinoma cells, and T98G and U373 human glioblastoma cells (**Figures 1G** and **S1C-D**). Comparatively, siLDHB did not affect the number of normal differentiated BJ human skin fibroblasts, HUVEC human umbilical vein endothelial cells and MCF10A human mammary gland epithelial cells (**Figures 1H** and **S1E**). However, the number of fetal HLF-1 fibroblasts was decreased by siLDHB. These observations justified further molecular investigation.

Targeting LDHB selectively inhibits basal autophagic flux in oxidative cancer cells

In oxidative cancer cells, the oxidative use of lactate preferentially to glucose could mimic glucose deprivation (Sonveaux et al., 2008; Leite et al., 2011), and glucose deprivation stimulates autophagy. Because unlike normal cells most cancer cells have a high level of basal autophagy (White, 2012; Avalos et al., 2014), we hypothesized that LDHB could control autophagy in cancer. To test this hypothesis, we first investigated combinations of siLDHB with known inhibitors of autophagy: chloroquine (Maclean et al., 2008) and a siRNA targeting ULK1 (siULK1), a serine/threonine-protein kinase that activates autophagy by phosphorylating beclin-1 (Russell et al., 2013). Individually,

siLDHB decreased SiHa cell number as efficiently as chloroquine (**Figures 2A, S2A-B**) and siULK1 (**Figure 2B**). There was no additive effect when combining siLDHB with chloroquine or with siULK1, indicating that these inhibitors target the same biological pathway. siLDHB and siULK1 were also equally potent and had no additive effects when used in combination in HeLa oxidative cervix cancer cells (**Figure S2C**). We further verified in both cell lines that siLDHB did not influence ULK1 and that siULK1 did not influence LDHB protein expression (**Figure S2D**). Similar to chloroquine, siLDHB induced both pro-apoptotic (**Figures 2C-D**) and antiproliferative (**Figure 2E**) effects on SiHa cells.

To demonstrate that LDHB controls autophagy in cancer cells, we first determined the abundance of LC3-II, a protein recruited to autophagic vesicles and a marker of the autophagic flux (Rubinsztein et al., 2009). Silencing LDHB induced leupeptin-sensitive LC3-II protein accumulation in SiHa cells (**Figures 2F** and **S2E**), which represented a potent inhibition of the autophagic flux (1.67 to 0.70) (**Figure 2F**), and was associated with accumulation of autophagic substrate optineurin (Korac et al., 2013) (**Figure 2G**). Similar data were obtained using HeLa cells, where autophagic LC3-II flux decreased (**Figure S2F**) and optineurin degradation was prevented (**Figure S2G**) by siLDHB.

Next, we tested the selectivity of LDHB versus LDHA in promoting autophagy in cancer cells. Having verified that siLDHB did not alter LDHA expression in SiHa cells (**Figure S2A**), we repeated autophagic flux experiments using a siRNA targeting LDHA (**Figure S2H**). siLDHA did not decrease SiHa cell number (**Figure 2H**) and did not alter the autophagic flux determined with LC3-II (**Figure 2I**) and optineurin (**Figure 2J**). Similarly, siLDHB did not alter LDHA expression in HeLa cells (**Figure S1C**) and siLDHA had no effect on the autophagic flux of these cells (**Figures S2H-J**). Together, these data demonstrate that LDHB but not LDHA controls the basal autophagic flux of oxidative cancer cells.

The control of basal autophagy by LDHB was selective to cancer cells, as siLDHB did not repress the growth and autophagic flux of nonmalignant BJ, HUVEC and MCF10A cells, to the exception of fetal HFL-1 fibroblasts (**Figures S2K-L**). It was confirmed using a second siRNA and doxycycline-induced shLDHB-1 that did not increase the abundance of optineurin except in HFL-1 fibroblasts (**Figure S1E** and **S2M-P**). Chloroquine caused optineurin accumulation only in HFL-1 fibroblasts, resulting in cell death (**Figures S2N&P**); it also reduced the number of MCF10A cells, but independently of optineurin accumulation (**Figures S2M&O**).

LDHB controls autophagic vesicle maturation

To understand how LDHB regulates autophagy, we examined vesicle trafficking. During autophagy, lysosomes fuse with autophagosomes to form autolysosomes containing active proteases. LDHB was expressed in the lysosomal fraction of SiHa cells (**Figure 3A**). Silencing of LDHB caused the accumulation of vesicles (**Figure 3B**) that were acidic (**Figure 3C**) and expressed the lysosomal marker LAMP-1 (**Figure 3D**). Acidic vesicle accumulation was also observed with chloroquine, with no additive effects of siLDHB on chloroquine (**Figure 3C**), suggesting that both treatments induce a lysosomal dysfunction that results in lysosome accumulation. Overexpressing LDHB had the opposite effect: it decreased the number of acidic vesicles per cell (**Figures 3C** and **S3A**). Of note, siLDHB did not affect the subcellular distribution pattern of lysosomes (distance to cell nucleus, **Figure 3E**).

Because there was no additive effect of siLDHB on the genetic disruption of autophagy by siULK1 that targets an early step of autophagy (**Figure 2B**) and no additive effect of siLDHB on autophagy inhibition by chloroquine that inhibits lysosomal activity (**Figure 2A**), we hypothesized that LDHB controls autophagic vesicle maturation. Accordingly, siLDHB repressed the fusion between lysosomes and autophagosomes, which was evidenced by a decrease in the number of vesicles that

coexpressed LAMP-1 and LC3 (**Figure 3F**). Similarly to chloroquine, siLDHB also decreased the abundance of mature autolysosomes measured using a LC3-mRFP-GFP reporter (Kimura et al., 2007) (**Figure 3G**). Defective fusion was associated with the accumulation of lysosomes (**Figure 3D**) and LC3-positive autophagosomes (**Figure 3H**). siLDHB decreased intracellular proteolysis, which was evidenced by decreased DQ-BSA dequenching (**Figure 3I** and **Figure S3B**) cells, whereas the early endocytic pathway was intact (**Figure S3C**).

Together, these data show that siLDHB induces lysosomal inhibition in oxidative cancer cells, thus positioning LDHB as an important contributor to lysosomal activity. This conclusion is supported by the fact that LDHB overexpression increased mature autolysosome formation (**Figures 3J** and **S3D**) and intracellular proteolysis (**Figures 3K** and **S3E**) in SiHa and in HeLa cells.

LDHB actively controls lysosomal activity in oxidative cancer cells

To test whether LDHB controls the lysosomal function through its enzymatic activity, we first produced vectors encoding HA-tagged catalytically inactive halves of the protein (hLDHBΔ163-331 and hLDHBΔ1-162). While re-expressing full-length LDHB effectively restored the number of SiHa cells transfected with a siRNA targeting the 5'-untranslated sequence of *LDHB* mRNA, neither hLDHBΔ163-331 nor hLDHBΔ1-162 restored cell number (**Figures 4A** and **S4A-B**). LDHB overexpression enhanced siCTR cell number. In addition, the MCT1 inhibitor α-cyano-4-hydroxycinnamate (CHC), known to inhibit lactate uptake in SiHa cells (Sonveaux et al., 2008), decreased cell number with no additional effect of siLDHB (**Figure 4B**). We therefore hypothesized that the enzymatic activity of LDHB promotes lysosome activity.

Upon glucose starvation, a condition stimulating autophagy and increasing lysosomal proteolysis in SiHa cells (**Figure S4C**), siLDHB decreased SiHa cell number (**Figure 4C**). Conversely,

delivering exogenous lactate activated intracellular proteolysis in glucose-starved (**Figure 4D**) and in glucose-replenished cells (**Figure 4E**). Lactate activated intracellular proteolysis in a LDHB-dependent manner (**Figure 4E**), indicating that lactate oxidation to pyruvate supports autophagy in oxidative cancer cells. Accordingly, lactate triggered autolysosome formation (**Figure 4F**), whereas CHC caused LC3-II protein accumulation with no additive effect on siLDHB (**Figure 4G**).

To fully understand the molecular determinants responsible for the control of autophagy by LDHB, we aimed to metabolically restore autophagy in LDHB-depleted SiHa cells. LDHB reaction substrate lactate and product pyruvate did not restore intracellular proteolysis (**Figures 4E&H**), but LDHB-depleted cells had switched to a glycolytic metabolism (**Figures S4D-E**), which, similar to MCT1 inhibition (Sonveaux et al., 2008), can oppose lactate and pyruvate uptake. However, neither cell-permeable methyl-lactate nor methyl-pyruvate restored cell number (**Figure S4F**) or acidic vesicle compartment size (**Figure S4G**), indicating that pyruvate downstream of LDHB does not promote autophagy. We therefore focused on the conversion of NAD^+ to NADH + H^+ associated with the oxidation of lactate by LDHB. While lactate induced MCT1-dependent lysosome acidification in the presence of LDHB (**Figure 4I**), siLDHB decreased the NADH/NAD^+ ratio (**Figure 4J**), which was associated with lysosome alkalinization (**Figures 4K** and **S4H&I**) but unchanged cytosolic pH (**Figure 4L**). Thus, the LDHB reaction promotes lysosomal acidification.

LDHB promotes V-ATPase-dependent lysosomal acidification

V-ATPase is the major contributor to lysosome acidification, with two protons translocated for each ATP hydrolyzed (Beyenbach and Wieczorek, 2006). Having found by proximity ligation assay that LDHB is in close proximity with V-ATPase (**Figure 5A**), we used co-immunoprecipitation and identified a physical interaction between LDHB and V-ATPase (**Figure 5B**). The V-ATPase inhibitor

bafilomycin A1 prevented the lysosomal acidification induced by LDHB overexpression (**Figure 5C** and **Figure S5A**), indicating that LDHB promotes V-ATPase-dependent lysosomal acidification. Main active proteases in SiHa cells are cysteine cathepsins B (**Figure S5B**), the acid-dependent cleavage/activation of which was also repressed by siLDHB (**Figure 5D**). This observation explains why lactate promotes and siLDHB decreases intracellular proteolysis.

Interestingly, silencing LDHB decreased the number of all the human cancer cell lines that we tested (**Figure 1G**), including WiDr human colon cancer cells that are aerobically glycolytic (Warburg effect) (Sonveaux et al., 2008). Therefore, using an isogenic series of cancer cells with different, previously characterized metabolic activities (Porporato et al., 2014), we finally aimed to test whether LDHB also controls lysosomal activity in glycolytic cancer cells that do not metabolically depend on lactate oxidation for ATP production (Sonveaux et al., 2008). siLDHB decreased the number of mitochondria-deficient SiHa-ρ0 cells (**Figures 5E** and **S5C**) and induced acidic vesicle accumulation (**Figure 5F**). In addition, siLDHA also decreased the number of glycolytic SiHa-ρ0 cells with no additive effect of chloroquine (**Figures 5G** and **S5C**), but not the number of wild-type oxidative SiHa cells (**Figure 2H**). These results indicate that glycolytic cancer cells use lactate-pyruvate cycling to maintain high lysosomal activity whereas oxidative cancer cells would use extracellular lactate delivered from the glycolytic tumor compartment to support autophagy (**Figure 5H)**.

Finally, we confirmed the therapeutic potential of targeting LDHB in cancer by comparing the antitumor efficacy of chloroquine and TET-on shLDHB-1 and shLDHB-3 on established HCT116 tumors in mice, thus using the same model as in **Figures S1A-B** but with two other shRNAs. Chloroquine and/or doxycycline were administered 13 days after tumor implantation once tumors reached 5 mm diameter. Silencing LDHB with shLDHB-1 or shLDHB-3 was more potent to retard HCT116 tumor growth than chloroquine delivered at a dose of 25 mg/kg every 3 days, and chloroquine

did not significantly enhance the effects of shLDHB-1 and shLDHB-3 (**Figure 5I**). Analysis of tumor biopsies at the end of the treatments confirmed that the two shRNAs inhibited autophagy in vivo, as they reduced the level of ATG12 (**Figures 5J&K**), which is involved in autophagosome formation (Geng and Klionsky, 2008) and is decreased when autophagy is blocked (Ciccia et al., 2014; Aravindan et al., 2015). Conversely, tumors expressing shLDHB significantly accumulated LC3-II (**Figure 5L**), with an increased number of LC3 foci in cancer cells (**Figure 5M**), and accumulated optineurin (**Figure S5G**), indicating a blockage in the degradation process. These differences were not seen when autophagy was inhibited by chloroquine treatment in mice (**Figures 5J-M** and **S5D-G**). Together, our results demonstrate that LDHB is a credible target for autophagy inhibition in cancer.

DISCUSSION

Our study positions LDHB as a key contributor to lysosomal activity and autophagy in cancer. Lysosomal acidification depends on LDHB activity both in oxidative and in glycolytic cancer cells, and silencing LDHB selectively inhibits the proliferation of cancer compared to normal differentiated cells, thus unraveling LDHB as a promising anticancer target. For therapy, LDHB inhibitors would offer a targeted and more selective alternative to the lysosomotropic agent chloroquine and its derivatives that act as weak bases. Indeed, chloroquine exerts side effects that are independent of autophagy inhibition (Maycotte et al., 2012; Maes et al., 2014), and its activity decreases with tumor acidity (Pellegrini et al., 2014).

LDHB is a key component of the oxidative pathway of lactate that controls metabolic cooperativeness between glycolytic and oxidative cancer cells (Sonveaux et al., 2008; Leite et al., 2011). In the metabolic cooperation based on the exchange of lactate, getting access to glucose is a clear metabolic advantage for glycolytic cancer cells. In turn, we report that oxidative cancer cells using lactate preferentially to glucose get a high autophagic flux as a metabolic reward. Mutual benefit resulting from lactate exchanges between different types of cancer cells substantiates the hypothesis of a metabolic symbiosis (Sonveaux et al., 2008) (**Figure 5H**). According to the extended version of the model, lactate produced glycolytically diffuses to the oxidative tumor cell compartment, enters into oxidative cancer cells preferentially via MCT1, and lactate and NAD^+ are converted to pyruvate, NADH and H^+ by LDHB. While pyruvate and NADH fuel oxidative mitochondrial metabolism (Sonveaux et al., 2008; Van Hee et al., 2015), LDHB promotes V-ATPase-dependent lysosomal acidification and autophagy, which is facilitated by a close interaction between LDHB and V-ATPase at the lysosomal surface. In oxygenated cancer cells that rapidly oxidize lactate, a high autophagic flux would primarily facilitate the recycling of damaged components (Rabinowitz and White, 2010). High

oxidative activities are indeed associated with elevated oxidative stress, and a major function of autophagy is to recycle oxidized proteins and organelles (Navarro-Yepes et al., 2014).

In oxidative cancer cells, LDHB couples lactate oxidation to autophagy not only when extracellular lactate is provided at a clinically relevant concentration (Walenta and Mueller-Klieser, 2004) (lactate-induced autophagy), but also under basal conditions when low levels of lactate are available (basal autophagy). Comparatively, glycolytic cancer cells generate high amounts of lactate from pyruvate intracellularly (the LDHA reaction). Lactate can either be exported (primarily via MCT4) to support metabolic symbiosis, or it can be oxidized back to pyruvate by LDHB (**Figure 5H**). At a first glance, this could be seen as a futile cycle, but it is not. LDHB is indeed needed to sustain autophagy and glycolytic cancer cell survival. In the process, similar to what happens in oxidative cancer cells, lactate and NAD^+ are converted to pyruvate, NADH and H^+ by LDHB. LDHB promotes V-ATPase-dependent lysosomal acidification and autophagy which, in these cells that often reside in metabolically restricted microenvironments, would constitute an additional source of energetic and biosynthetic precursors (Rabinowitz and White, 2010). Transferring protons to lysosomes could also contribute to the pH homeostasis of the cytosol (Spugnini et al., 2014).

Blocking basal autophagy can kill cancer cells (Avalos et al., 2014), and we report that silencing LDHB inhibits basal autophagy, cancer cell proliferation and induces apoptotic cell death. Three characteristics of the response are remarkable. First, silencing LDHB is as effective as chloroquine in inhibiting autophagy. Second, silencing LDHB generally impairs the expansion of human cancer cell lines. Of note, we found that MCF7 cells that are relatively non-dependent on autophagy (Yang et al., 2011; Mancias et al., 2014; Maycotte et al., 2014) are the least sensitive; and autophagy-dependent, Ras-mutated HCT116 cells (Guo et al., 2011) the most sensitive to LDHB silencing. Third, silencing LDHB shows selectivity for cancer versus normal differentiated cells. Thus,

compared to chloroquine and its derivatives that are currently undergoing clinical trials but act in a non-targeted and non-specific manner, targeting LDHB could offer a unique opportunity to inhibit a precise target controlling lysosomal activity and autophagy preferentially in cancer cells. Compared to other components of lactate metabolism, we propose LDHB as a preferred target to simultaneously inhibit autophagy in glycolytic and oxidative cancer cells. In comparison, inhibiting LDHA or MCT4 would decrease the autophagic flux only in glycolytic cancer cells, and targeting MCT1 would block autophagy only in oxidative cancer cells. In support of this, LDHB is an independent prognostic marker of overall survival in uterine cancer patients and promotes the progression of several different types of tumors (De Haas et al., 2008; Yoo et al., 2009; Hussien and Brooks, 2011; Isozaki et al., 2012; McCleland et al., 2012; Beronja et al., 2013; Dennison et al., 2013; Koshiyama et al., 2013; McCleland et al., 2013). Previous studies further indicated that complete hereditary deficiency of LDHB has no symptomatic consequences in humans (Okumura et al., 1999; Sudo et al., 1999), thus supporting the future clinical development of pharmacological inhibitors of LDHB.

Similarly to other inhibitors of autophagy that display most of their therapeutic activity in combination with other anticancer therapies (Chen and Karantza-Wadsworth, 2009; Chen et al., 2010; Amaravadi et al., 2011), silencing LDHB had only limited effects at the beginning of tumor progression, but stronger effects were seen when silencing was induced at a later time point. Resistance is unlikely to arise from LDHB re-expression or an expressional compensation by LDHA, but could potentially result from metabolic adaptations, in particular switching to a more glycolytic metabolism in an aerobic environment in order to compensate for autophagy inhibition (White, 2012).

Conclusively, we believe that the identification that lactate and LDHB control lysosomal activity and autophagy preferentially in cancer cells lays the ground for promising anticancer applications.

EXPERIMENTAL PROCEDURES

Patient database analysis

The SurvExpress gene expression database (Aguirre-Gamboa et al., 2013) was used for the analysis of overall survival in Uterine Corpus Endometrioid Carcinoma TCGA (332 samples). Patients were classified into two risk groups according to gene expression and censored for overall survival without stratification.

In vivo experiments

All in vivo experiments were performed with approval of UCL *Comité d'Ethique pour l'Expérimentation Animale* (approval ID: TUMETABO) according to national and European animal care regulations. Tumor generation with SiHa and with HCT116 cells expressing shCTR or shLDHB-1 and growth rate determination were conducted as previously described (De Saedeleer et al., 2012). A detailed description of the experimental procedures is provided in Supplemental Experimental Procedures.

Cells and reagents

All cell lines were from ATCC, except SKOV3 human ovarian carcinoma cells (Wintzell et al., 2012), T98G and U373 human glioblastoma cells (Bruyere et al., 2011), and human umbilical vein endothelial cells (HUVEC, Sigma-Aldrich). Details on culture conditions are provided in Supplemental Experimental Procedures. Unless stated otherwise, all chemicals were from Sigma-Aldrich. To avoid changes in extracellular pH, lactate and pyruvate were used as sodium salts or methylated cell-permeable forms. For functional assays, all data were normalized for cell number or total protein content.

Cell number, proliferation and apoptosis

Cell number and cell death were measured using trypan blue exclusion on a NucleoCounter device (ChemoMetec). Apoptosis was assayed by measuring caspase-3 (Casp3) cleavage using western blotting. Cell proliferation was evaluated by immunocytochemistry using a mouse monoclonal antibody against Ki-67 (556003, BD Biosciences), and expressed as the percentage of Ki-67-positive cells under total nuclei count on thresholded images using ImageJ software 1.46r.

RNA interference and cell transfection

shRNAs were delivered with lentiviruses, and siRNAs and plasmids using transfection. Details are provided in Supplemental Experimental Procedures.

Co-immunoprecipitation and Western blotting

Co-immunoprecipitation was performed using Dynabeads protein G (Invitrogen) according to manufacturer's protocol. Immunoblotting was performed as previously described (Feron et al., 1996). Details are provided in Supplemental Experimental Procedures.

Immunochemistry and proximity ligation assay

Immunohistochemistry and immunocytofluorescence labeling were performed as previously described (Sonveaux et al., 2008). *In situ* protein-protein interactions were detected using the proximity ligation assay (PLA, Duolink kit) of Olink Bioscience according to the manufacturer's instructions. Details are provided in Supplemental Experimental Procedures.

Cell fractionation

Cells fractionation was performed according to (Schroter et al., 1999). The procedures are detailed in Supplemental Experimental Procedures.

Electron microscopy

Transmission electron microscopy was performed using a previously described protocol (Piret et al., 2012).

Endosome, lysosome and autophagic assays

Endocytic trafficking was measured using a previously described transferrin recycling assay (Magadan et al., 2006). Intracellular proteolysis was quantified based on the intracellular degradation of fluorogenic substrate DQ green BSA (Invitrogen). Acidic vesicles were determined using acridine orange (Sigma) fluorescence measurements, lysosomal pH after the overnight endocytosis of 0.5 mg/ml pH sensitive FITC-dextran (Sigma) by intact cells (Vidal-Donet et al., 2013), and autophagosome maturation with a mRFP-GFP-LC3-encoding construct (Plasmid 21074: ptfLC3, Addgene) used according to (Kimura et al., 2007). Cytosolic pH was measured using SNARF-1-AM. Details are provided in Supplemental Experimental Procedures.

Metabolic assays

For metabolic assays, an equal number of cells were plated in 6-well plates in fresh medium. Seventy-two hours later, glucose and lactate concentrations were measured in deproteinized cell supernatants using specific enzymatic assays on a CMA600 Microdialysis Analyzer (CMA microdialysis). Data were normalized by final cell numbers.

LDHB activity

LDHB activity was measured in intact cells using the NADH/NAD^+ ratio that was quantified in clear cell lysates using the NAD/NADH Quantitation Kit from Source Bioscience according to the manufacturers' instructions. In cell lysates, measurements of LDHB activity were performed using the Lactate dehydrogenase B activity assay kit (Abcam) following the manufacturer's instructions.

Statistics

All data are normalized to control and are presented as means ± SEM. *n* corresponds to the number of independent experiments. In some figures, SEM are smaller than symbols. Two-tailed unpaired Student's *t* test, Mann Whitney test, Wilcoxon Signed Rank test, one-way ANOVA followed by Holm-Sidak's multiple comparison test, Kruskal-Wallis followed by Dunn's multiple comparison test and two-way ANOVA were used where appropriate. A LogRank test was used to compare survival curves. $p < 0.05$ was considered to be statistically significant. Methods and any associated references are available in the online version of the paper.

SUPPLEMENTAL INFORMATION

Supplemental Information includes five figures and Supplemental Experimental Procedures, and can be found with this article online.

AUTHOR CONTRIBUTIONS

L.B. conducted all experiments. L.B., P.B., M.S., P.D., V.V.H., J.F., C.B., P.E.P., T.C. and P.S. designed protocols. L.B., P.B., C.D., P.D., M-J.F., V.V.H., T.V., M.T., J.F., C.B., C.M. and T.C. performed experiments and analyzed data. T.C. produced LDHB plasmid constructs. L.B., T.C., R.F. and P.S. designed constructs derived from LDHB. L.B. and P.S. wrote the manuscript. L.B., P.B., M.S., C.D., P.D., M-J.F., V.V.H., T.V., M.T., J.F., C.B., P.E.P., R.F., C.M., T.C. and P.S. edited and approved the manuscript. P.S. obtained all grants and supervised the study.

ACKNOWLEDGEMENTS

This work was supported by ERC Starting Grant No. 243188 TUMETABO, IAP grant #UP7-03 from the Belgian Science Policy Office (Belspo), an *Action de Recherche Concertée* from the *Communauté Française de Belgique* (ARC 14/19-058), the Belgian *Fonds National de la Recherche Scientifique* (F.R.S.-FNRS), the Belgian *Fondation contre le Cancer* (2012-186), and the UCL *Fonds Spéciaux de la Recherche* (FSR). P.S. is a F.R.S.-FNRS Research Associate, and P.E.P, P.B. and P.D. are F.R.S.-FNRS Postdoctoral Fellows. M.S. and V.V.H. are *Télévie* Research Fellows. We thank Chantal Fregimilicka and Valéry L Payen for excellent technical assistance, Maria Shoshan (Karolinska Institute, Sweden) for the gift of SKOV3 cells, Florence Lefranc (ULB, Belgium) for T98G and U373 cells and Dominique Lison (UCL) for HFL-1 cells; and the morphology and electron microscopy services of UNamur for electron microscopy analyses.

REFERENCES

Aguirre-Gamboa, R., Gomez-Rueda, H., Martinez-Ledesma, E., Martinez-Torteya, A., Chacolla-Huaringa, R., Rodriguez-Barrientos, A., Tamez-Pena, J.G., and Trevino, V. (2013). SurvExpress: an online biomarker validation tool and database for cancer gene expression data using survival analysis. PLoS. ONE. *8*, e74250.

Amaravadi, R.K., Lippincott-Schwartz, J., Yin, X.M., Weiss, W.A., Takebe, N., Timmer, W., Dipaola, R.S., Lotze, M.T., and White, E. (2011). Principles and current strategies for targeting autophagy for cancer treatment. Clin. Cancer Res. *17*, 654-666.

Aravindan, S., Ramraj, S.K., Somasundaram, S.T., and Aravindan, N. (2015). Novel adjuvants from seaweed impede autophagy signaling in therapy-resistant residual pancreatic cancer. J. Biomed. Sci. *22*, 28.

Avalos, Y., Canales, J., Bravo-Sagua, R., Criollo, A., Lavandero, S., and Quest, A.F. (2014). Tumor Suppression and Promotion by Autophagy. Biomed. Res. Int. *2014*, 603980.

Beronja, S., Janki, P., Heller, E., Lien, W.H., Keyes, B.E., Oshimori, N., and Fuchs, E. (2013). RNAi screens in mice identify physiological regulators of oncogenic growth. Nature *501*, 185-190.

Beyenbach, K.W., and Wieczorek, H. (2006). The V-type H+ ATPase: molecular structure and function, physiological roles and regulation. J. Exp. Biol. *209*, 577-589.

Bruyere, C., Abeloos, L., Lamoral-Theys, D., Senetta, R., Mathieu, V., Le, M.M., Kast, R.E., Cassoni, P., Vandenbussche, G., Kiss, R. et al. (2011). Temozolomide modifies caveolin-1 expression in experimental malignant gliomas in vitro and in vivo. Transl. Oncol. *4*, 92-100.

Chen, N., and Karantza-Wadsworth, V. (2009). Role and regulation of autophagy in cancer. Biochim. Biophys. Acta *1793*, 1516-1523.

Chen, S., Rehman, S.K., Zhang, W., Wen, A., Yao, L., and Zhang, J. (2010). Autophagy is a therapeutic target in anticancer drug resistance. Biochim. Biophys. Acta *1806*, 220-229.

Ciccia, F., Accardo-Palumbo, A., Rizzo, A., Guggino, G., Raimondo, S., Giardina, A., Cannizzaro, A., Colbert, R.A., Alessandro, R., and Triolo, G. (2014). Evidence that autophagy, but not the unfolded protein response, regulates the expression of IL-23 in the gut of patients with ankylosing spondylitis and subclinical gut inflammation. Ann. Rheum. Dis. *73*, 1566-1574.

Commisso, C., Davidson, S.M., Soydaner-Azeloglu, R.G., Parker, S.J., Kamphorst, J.J., Hackett, S., Grabocka, E., Nofal, M., Drebin, J.A., Thompson, C.B. et al. (2013). Macropinocytosis of protein is an amino acid supply route in Ras-transformed cells. Nature *497*, 633-637.

Curry, J.M., Tuluc, M., Whitaker-Menezes, D., Ames, J.A., Anantharaman, A., Butera, A., Leiby, B., Cognetti, D.M., Sotgia, F., Lisanti, M.P. et al. (2013). Cancer metabolism, stemness and tumor recurrence: MCT1 and MCT4 are functional biomarkers of metabolic symbiosis in head and neck cancer. Cell Cycle *12*, 1371-1384.

De Saedeleer, C.J., Copetti, T., Porporato, P.E., Verrax, J., Feron, O., and Sonveaux, P. (2012). Lactate activates HIF-1 in oxidative but not in Warburg-phenotype human tumor cells. PLoS. ONE. *7*, e46571.

De Haas, H.T., Hasselt, N., Troost, D., Caron, H., Popovic, M., Zadravec-Zaletel, L., Grajkowska, W., Perek, M., Osterheld, M.C., Ellison, D. et al. (2008). Molecular risk stratification of medulloblastoma patients based on immunohistochemical analysis of MYC, LDHB, and CCNB1 expression. Clin. Cancer Res. *14*, 4154-4160.

Dennison, J.B., Molina, J.R., Mitra, S., Gonzalez-Angulo, A.M., Balko, J.M., Kuba, M.G., Sanders, M.E., Pinto, J.A., Gomez, H.L., Arteaga, C.L. et al. (2013). Lactate dehydrogenase B: a metabolic marker of response to neoadjuvant chemotherapy in breast cancer. Clin. Cancer Res. *19*, 3703-3713.

Dewhirst, M.W., Cao, Y., and Moeller, B. (2008). Cycling hypoxia and free radicals regulate angiogenesis and radiotherapy response. Nat. Rev. Cancer *8*, 425-437.

Dhup, S., Dadhich, R.K., Porporato, P.E., and Sonveaux, P. (2012). Multiple biological activities of lactic acid in cancer: influences on tumor growth, angiogenesis and metastasis. Curr. Pharm. Des *18*, 1319-1330.

Feron, O., Belhassen, L., Kobzik, L., Smith, T.W., Kelly, R.A., and Michel, T. (1996). Endothelial nitric oxide synthase targeting to caveolae. Specific interactions with caveolin isoforms in cardiac myocytes and endothelial cells. J. Biol. Chem. *271*, 22810-22814.

Guillaumond, F., Leca, J., Olivares, O., Lavaut, M.N., Vidal, N., Berthezene, P., Dusetti, N.J., Loncle, C., Calvo, E., Turrini, O. et al. (2013). Strengthened glycolysis under hypoxia supports tumor symbiosis and hexosamine biosynthesis in pancreatic adenocarcinoma. Proc. Natl. Acad. Sci. U. S. A *110*, 3919-3924.

Guo, J.Y., Chen, H.Y., Mathew, R., Fan, J., Strohecker, A.M., Karsli-Uzunbas, G., Kamphorst, J.J., Chen, G., Lemons, J.M., Karantza, V. et al. (2011). Activated Ras requires autophagy to maintain oxidative metabolism and tumorigenesis. Genes Dev. *25*, 460-470.

Halestrap, A.P., and Wilson, M.C. (2012). The monocarboxylate transporter family--role and regulation. IUBMB. Life *64*, 109-119.

Hanahan, D., and Weinberg, R.A. (2011). Hallmarks of cancer: the next generation. Cell *144*, 646-674.

Hensley, C.T., Wasti, A.T., and DeBerardinis, R.J. (2013). Glutamine and cancer: cell biology, physiology, and clinical opportunities. J. Clin. Invest *123*, 3678-3684.

Ho, J., de Moura, M.B., Lin, Y., Vincent, G., Thorne, S., Duncan, L.M., Hui-Min, L., Kirkwood, J.M., Becker, D., Van, H.B. et al. (2012). Importance of glycolysis and oxidative phosphorylation in advanced melanoma. Mol. Cancer *11*, 76.

Hussien, R., and Brooks, G.A. (2011). Mitochondrial and plasma membrane lactate transporter and lactate dehydrogenase isoform expression in breast cancer cell lines. Physiol Genomics *43*, 255-264.

Icard, P., Kafara, P., Steyaert, J.M., Schwartz, L., and Lincet, H. (2014). The metabolic cooperation between cells in solid cancer tumors. Biochim. Biophys. Acta *1846*, 216-225.

Isozaki, Y., Hoshino, I., Nohata, N., Kinoshita, T., Akutsu, Y., Hanari, N., Mori, M., Yoneyama, Y., Akanuma, N., Takeshita, N. et al. (2012). Identification of novel molecular targets regulated by tumor suppressive miR-375 induced by histone acetylation in esophageal squamous cell carcinoma. Int. J. Oncol. *41*, 985-994.

Kennedy, K.M., Scarbrough, P.M., Ribeiro, A., Richardson, R., Yuan, H., Sonveaux, P., Landon, C.D., Chi, J.T., Pizzo, S., Schroeder, T. et al. (2013). Catabolism of exogenous lactate reveals it as a legitimate metabolic substrate in breast cancer. PLoS. ONE. *8*, e75154.

Kimura, S., Noda, T., and Yoshimori, T. (2007). Dissection of the autophagosome maturation process by a novel reporter protein, tandem fluorescent-tagged LC3. Autophagy. *3*, 452-460.

Korac, J., Schaeffer, V., Kovacevic, I., Clement, A.M., Jungblut, B., Behl, C., Terzic, J., and Dikic, I. (2013). Ubiquitin-independent function of optineurin in autophagic clearance of protein aggregates. J. Cell Sci. *126*, 580-592.

Koshiyama, A., Ichibangase, T., and Imai, K. (2013). Comprehensive fluorogenic derivatization-liquid chromatography/tandem mass spectrometry proteomic analysis of colorectal cancer cell to identify biomarker candidate. Biomed. Chromatogr. *27*, 440-450.

Krajcovic, M., and Overholtzer, M. (2012). Mechanisms of ploidy increase in human cancers: a new role for cell cannibalism. Cancer Res. *72*, 1596-1601.

Leite, T.C., Coelho, R.G., Da Silva, D., Coelho, W.S., Marinho-Carvalho, M.M., and Sola-Penna, M. (2011). Lactate downregulates the glycolytic enzymes hexokinase and phosphofructokinase in diverse tissues from mice. FEBS Lett. *585*, 92-98.

Levine, B., and Kroemer, G. (2008). Autophagy in the pathogenesis of disease. Cell *132*, 27-42.

Maclean, K.H., Dorsey, F.C., Cleveland, J.L., and Kastan, M.B. (2008). Targeting lysosomal degradation induces p53-dependent cell death and prevents cancer in mouse models of lymphomagenesis. J. Clin. Invest *118*, 79-88.

Maes, H., Kuchnio, A., Peric, A., Moens, S., Nys, K., De, B.K., Quaegebeur, A., Schoors, S., Georgiadou, M., Wouters, J. et al. (2014). Tumor vessel normalization by chloroquine independent of autophagy. Cancer Cell *26*, 190-206.

Magadan, J.G., Barbieri, M.A., Mesa, R., Stahl, P.D., and Mayorga, L.S. (2006). Rab22a regulates the sorting of transferrin to recycling endosomes. Mol. Cell Biol. *26*, 2595-2614.

Mancias, J.D., Wang, X., Gygi, S.P., Harper, J.W., and Kimmelman, A.C. (2014). Quantitative proteomics identifies NCOA4 as the cargo receptor mediating ferritinophagy. Nature *509*, 105-109.

Maycotte, P., Aryal, S., Cummings, C.T., Thorburn, J., Morgan, M.J., and Thorburn, A. (2012). Chloroquine sensitizes breast cancer cells to chemotherapy independent of autophagy. Autophagy. *8*, 200-212.

Maycotte, P., Gearheart, C.M., Barnard, R., Aryal, S., Mulcahy Levy, J.M., Fosmire, S.P., Hansen, R.J., Morgan, M.J., Porter, C.C., Gustafson, D.L. et al. (2014). STAT3-mediated autophagy dependence identifies subtypes of breast cancer where autophagy inhibition can be efficacious. Cancer Res. *74*, 2579-2590.

Mazurek, S. (2011). Pyruvate kinase type M2: A key regulator of the metabolic budget system in tumor cells. Int. J. Biochem. Cell Biol. *43*, 969-980.

McCleland, M.L., Adler, A.S., Deming, L., Cosino, E., Lee, L., Blackwood, E.M., Solon, M., Tao, J., Li, L., Shames, D. et al. (2013). Lactate dehydrogenase B is required for the growth of KRAS-dependent lung adenocarcinomas. Clin. Cancer Res. *19*, 773-784.

McCleland, M.L., Adler, A.S., Shang, Y., Hunsaker, T., Truong, T., Peterson, D., Torres, E., Li, L., Haley, B., Stephan, J.P. et al. (2012). An integrated genomic screen identifies LDHB as an essential gene for triple-negative breast cancer. Cancer Res. *72*, 5812-5823.

Mullen, A.R., Wheaton, W.W., Jin, E.S., Chen, P.H., Sullivan, L.B., Cheng, T., Yang, Y., Linehan, W.M., Chandel, N.S., and DeBerardinis, R.J. (2012). Reductive carboxylation supports growth in tumour cells with defective mitochondria. Nature *481*, 385-388.

Navarro-Yepes, J., Burns, M., Anandhan, A., Khalimonchuk, O., del Razo, L.M., Quintanilla-Vega, B., Pappa, A., Panayiotidis, M.I., and Franco, R. (2014). Oxidative stress, redox signaling, and autophagy: cell death versus survival. Antioxid. Redox. Signal. *21*, 66-85.

Pellegrini, P., Strambi, A., Zipoli, C., Hagg-Olofsson, M., Buoncervello, M., Linder, S., and De Milito,.A. (2014). Acidic extracellular pH neutralizes the autophagy-inhibiting activity of chloroquine: implications for cancer therapies. Autophagy. *10*, 562-571.

Piret, J.P., Vankoningsloo, S., Mejia, J., Noel, F., Boilan, E., Lambinon, F., Zouboulis, C.C., Masereel, B., Lucas, S., Saout, C. et al. (2012). Differential toxicity of copper (II) oxide nanoparticles of similar hydrodynamic diameter on human differentiated intestinal Caco-2 cell monolayers is correlated in part to copper release and shape. Nanotoxicology. *6*, 789-803.

Porporato, P.E., Dadhich, R.K., Dhup, S., Copetti, T., and Sonveaux, P. (2011). Anticancer targets in the glycolytic metabolism of tumors: a comprehensive review. Front. Pharmacol. *2*, 49.

Porporato, P.E., Payen, V.L., Perez-Escuredo, J., De Saedeleer, C.J., Danhier, P., Copetti, T., Dhup, S., Tardy, M., Vazeille, T., Bouzin, C. et al. (2014). A mitochondrial switch promotes tumor metastasis. Cell Rep. *8*, 754-766.

Rabinowitz, J.D., and White, E. (2010). Autophagy and metabolism. Science *330*, 1344-1348.

Rubinsztein, D.C., Cuervo, A.M., Ravikumar, B., Sarkar, S., Korolchuk, V., Kaushik, S., and Klionsky, D.J. (2009). In search of an "autophagomometer". Autophagy. *5*, 585-589.

Russell, R.C., Tian, Y., Yuan, H., Park, H.W., Chang, Y.Y., Kim, J., Kim, H., Neufeld, T.P., Dillin, A., and Guan, K.L. (2013). ULK1 induces autophagy by phosphorylating Beclin-1 and activating VPS34 lipid kinase. Nat. Cell Biol. *15*, 741-750.

Schroter, C.J., Braun, M., Englert, J., Beck, H., Schmid, H., and Kalbacher, H. (1999). A rapid method to separate endosomes from lysosomal contents using differential centrifugation and hypotonic lysis of lysosomes. J. Immunol. Methods *227*, 161-168.

Sonveaux, P., Vegran, F., Schroeder, T., Wergin, M.C., Verrax, J., Rabbani, Z.N., De Saedeleer, C.J., Kennedy, K.M., Diepart, C., Jordan, B.F. et al. (2008). Targeting lactate-fueled respiration selectively kills hypoxic tumor cells in mice. J. Clin. Invest *118*, 3930-3942.

Spugnini E., Sonveaux P., Stock C.M., Perez-Sayans M., De Milito A., Avnet S., Garcia A.G., Harguidey S., and Fais S. (2014) Implication of proton channels and exchangers in cancer. BBA Biomembranes *1848*, 2715-2726.

Tan, A.S., Baty, J.W., Dong, L.F., Bezawork-Geleta, A., Endaya, B., Goodwin, J., Bajzikova, M., Kovarova, J., Peterka, M., Yan, B. et al. (2015). Mitochondrial genome acquisition restores respiratory function and tumorigenic potential of cancer cells without mitochondrial DNA. Cell Metab *21*, 81-94.

Van Hee V.F., Perez-Escuredo J., Cacace A., Copetti T., and Sonveaux P. (2015) Lactate does not activate NF-κB in oxidative tumor cells. Front Pharmacol *6*, 28.

Vidal-Donet, J.M., Carcel-Trullols, J., Casanova, B., Aguado, C., and Knecht, E. (2013). Alterations in ROS activity and lysosomal pH account for distinct patterns of macroautophagy in LINCL and JNCL fibroblasts. PLoS. ONE. *8*, e55526.

Walenta, S., and Mueller-Klieser, W.F. (2004). Lactate: mirror and motor of tumor malignancy. Semin. Radiat. Oncol. *14*, 267-274.

Walenta, S., Snyder, S., Haroon, Z.A., Braun, R.D., Amin, K., Brizel, D., Mueller-Klieser, W., Chance, B., and Dewhirst, M.W. (2001). Tissue gradients of energy metabolites mirror oxygen tension gradients in a rat mammary carcinoma model. Int. J. Radiat. Oncol. Biol. Phys. *51*, 840-848.

Warburg, O. (1956). On the origin of cancer cells. Science *123*, 309-314.

White, E. (2012). Deconvoluting the context-dependent role for autophagy in cancer. Nat. Rev. Cancer *12*, 401-410.

Wintzell, M., Lofstedt, L., Johansson, J., Pedersen, A.B., Fuxe, J., and Shoshan, M. (2012). Repeated cisplatin treatment can lead to a multiresistant tumor cell population with stem cell features and sensitivity to 3-bromopyruvate. Cancer Biol. Ther. *13*, 1454-1462.

Yang, S., Wang, X., Contino, G., Liesa, M., Sahin, E., Ying, H., Bause, A., Li, Y., Stommel, J.M., Dell'antonio, G. et al. (2011). Pancreatic cancers require autophagy for tumor growth. Genes Dev. *25*, 717-729.

Yoo, H.J., Yun, B.R., Kwon, J.H., Ahn, H.S., Seol, M.A., Lee, M.J., Yu, G.R., Yu, H.C., Hong, B., Choi, K. et al. (2009). Genetic and expression alterations in association with the sarcomatous change of cholangiocarcinoma cells. Exp. Mol. Med. *41*, 102-115.

Yoon, Y.H., Cho, K.S., Hwang, J.J., Lee, S.J., Choi, J.A., and Koh, J.Y. (2010). Induction of lysosomal dilatation, arrested autophagy, and cell death by chloroquine in cultured ARPE-19 cells. Invest Ophthalmol. Vis. Sci. *51*, 6030-6037.

FIGURE LEGENDS

Figure 1. Silencing LDHB delays tumor growth and decreases cancer cell number. (**A**) SurvExpress gene expression database analysis of potential markers of overall survival in uterine cancer patients (n = 332 patients in total; 164-168 patients per group). (**B**) Tumor growth of SiHa cancer cells carrying a TET-on control shRNA (shCTR) or a TET-on shRNA targeting LDHB (shLDHB-1) in mice treated with doxycycline (1 mg/ml) or vehicle via the drinking water starting 1 day after cell inoculation (n = 8 mice per group). (**C, D**) LDHB and LDHA protein expression (C) and cleaved caspase 3 (D) in the lysates of tumors collected from animals sacrificed at the end of the experiment (n = 8). (**E**) Immunohistochemical detection and quantification of proliferation marker Ki-67 in tumors treated with doxycycline collected at the end of the experiment shown in (B) (scale bar 1 mm on top panels and 200 μm in bottom panels; n = 8). (**F**) Representative western blots of SiHa cells harboring shCTR or shLDHB-1 treated with or without doxycycline (0.5 μg/ml) for 3 days and quantification on cell number after 3 and 10 days of treatment (n = 4). Results at day 10 involved replating an equal number of cells at day 7, then letting them grow for 3 more days. (**G**) Cancer cells were transfected with a control siRNA (siCTR) or with siRNAs against LDHB (siLDHB-1 or siLDHB-2) and counted 72 hr later (n = 3-4). (**H**) As in (G) but using nonmalignant cells (n = 4-6). All data represent means ± SEM. *$p < 0.05$, **$p < 0.001$ ***$p < 0.005$, ns, not significant, by LogRank test (**A**), two-way ANOVA (**B**), Mann Whitney test (**C**, **E**), Wilcoxon matched-pairs signed rank test (**D**), one-way ANOVA and Holm-Sidak's multiple comparison test (**F**) or two-tailed unpaired Student's t test (**G-H**). See also **Figure S1**.

Figure 2. Silencing LDHB inhibits autophagy in SiHa oxidative cancer cells. (**A**) Numbers of cells that were transfected for 72 hr with siCTR or siLDHB-1 and treated with or without 20 μM

chloroquine for the last 48 hr (n = 6). (**B**) Numbers of cells at 72 hr after transfection with siCTR, siLDHB, siULK1 or siLDHB + siULK1 (n = 5). (**C**) Cell death measured by trypan blue exclusion of cells transfected as indicated and then treated with or without 20 μM chloroquine for 48 hr (n = 9-12). (**D**) Representative western blot and quantification of cleaved caspase 3 of cells at 72 hr after transfection as indicated (n = 3). (**E**) Cell proliferation evaluated by Ki-67 staining in cells with transfection for 72 hr or treatment with or without 20 μM chloroquine for 48 hr as indicated (n = 3). (**F**) LDHB, LDHA, LC3-I and LC3-II protein expression in cells treated overnight with or without leupeptin (150 μM) (n = 13). Autophagic flux was calculated as the difference of LC3-II expression between conditions with and without leupeptin. (**G**) Optineurin protein expression in cells transfected with siCTR or siLDHB-1 (n = 8). (**H**) Number of cells 72 hr after transfection with siCTR or siLDHA (n = 6). (**I**) Western blot quantification of LDHA and LC3-II in cells transfected as indicated and treated overnight with or without leupeptin (150 μM) (n = 4). (**J**) Optineurin and LDHA protein expression (n = 4). All data represent means ± SEM. *p < 0.05, **p < 0.01, ***p < 0.005, ns, not significant, by one-way ANOVA and Holm-Sidak's multiple comparisons test (**A, B**), two-tailed unpaired Student's t test (**C**-**E**, **H**), Kruskal-Wallis and Dunn's multiple comparisons test (**F** middle, **I**) or Mann Whitney test (**F** right, **G**, **J**). See also **Figure S2**.

Figure 3. LDHB controls autophagic vesicle maturation. (**A**) Representative immunoblots of subcellular fractions of SiHa cells (n = 3). Rab4 and cathepsin B are used as marker enriched in the endosomal and lysosomal fractions, respectively. (**B**) Representative electron micrographs of SiHa cells transfected as indicated (scale bar 2 μm). (**C**) Acidic vesicle content measured using acridine orange staining in SiHa cells transfected as indicated and treated with or without 20 μM chloroquine for 48 hr (top graph, n = 4; bottom graph, n = 3). (**D**) Representative images of LAMP1

immunostaining and quantification of lysosome density in SiHa cells transfected as indicated (scale bar 20 µm, n = 3). (**E**) Quantification of lysosome distance to nucleus of images obtained in D (n = 3). (**F**) Evaluation of lysosome-autophagosome fusion in SiHa cells transfected as indicated using LAMP1 and LC3 immunostaining and Pearson correlation coefficient calculation. Closed and open arrows show mature and immature autophagosomes, respectively (scale bar 20 µm, n = 3). (**G**) The abundance of autophagosomes and autolysosomes was measured with a LC3-GFP-mRFP reporter in SiHa cells transfected or treated with or without 20 µM chloroquine for 48 hr as indicated (scale bar 10 µm, n = 4). (**H**) Representative images of LC3 immunostaining and quantification of LC3-positive vesicles in SiHa cells transfected or treated with or without 20 µM chloroquine for 48 hr as indicated (scale bar 10 µm, n = 3). (**I**) Representative images and quantification of intracellular proteolysis by DQ-BSA dequenching in SiHa cells treated ± 20 µM chloroquine for 48 hr (scale bar 20 µm, n = 3). (**J**) Autophagosomes and autolysosomes abundance measured with a LC3-GFP-mRFP reporter in SiHa cells 48 hr after transfection (n = 4). (**K**) Intracellular proteolysis measured with DQ-BSA in SiHa cells 48 hr after transfection (n = 3). All data represent means ± SEM. *$p < 0.05$, **$p < 0.01$, ***$p < 0.005$, ns, not significant, Kruskal-Wallis with Dunn's (**C**, **G**, **I**, **J**), Mann Whitney test (**C**, **K**), two-tailed unpaired Student's t test (**D-F**) or one-way ANOVA with Holm-Sidak's multiple comparisons test (**H**). See also **Figure S3**.

Figure 4. Lactate promotes LDHB-dependent autophagy in oxidative cancer cells. (**A**) Numbers of SiHa cells transfected with indicated siRNA without or with ectopic expression of LDHB, hLDHBΔ163-331 or hLDHBΔ1-162 (n = 5-7). (**B**) Numbers of SiHa cells transfected with indicated siRNA and then treated with or without 10 µM CHC for 48 hr (n = 6). (**C**) Number of SiHa cells transfected as indicated after glucose and serum starvation for 6 hr (n = 6). (**D-E**) Representative

images and quantification of intracellular proteolysis by DQ-BSA in SiHa cells grown without (D) or with (E) glucose and with or without treatment with 10 mM lactate (scale bars 20 μm, 48 hr treatment, n = 4 per group). (**F**) Abundance of autophagosomes and of autolysosomes measured with LC3-GFP-mRFP in SiHa cells treated with or without 10 mM lactate for 48 hr (scale bar 20 μm, n = 4). (**G**) LDHB, LC3-I and LC3-II protein abundance in SiHa cells treated with or without 10 μM CHC for 48 hr (n = 4). (**H**) Intracellular proteolysis in SiHa cells treated with or without 10 mM pyruvate for 48 hr (scale bar 20 μm, n = 3). (**I**) Lysosomal pH measured with FITC-dextran in SiHa cells treated with or without 10 mM sodium lactate together with or without 10 μM CHC for 48 hr (n = 4). (**J**) $NADH/NAD^+$ ratio measured enzymatically (n = 3). (**K**) Lysosomal pH (n = 4). (**L**) Intracellular pH measured with SNARF-1-AM (n = 4). All data represent means ± SEM. *p < 0.05, **p < 0.01, ***p < 0.005, ns, not significant, by one-way ANOVA with Holm-Sidak's multiple comparisons test (**A**, **B**, **I**), two-tailed unpaired Student's t test (**C**, **J**-**L**), Mann Whitney test (**D**), or Kruskal-Wallis with Dunn's multiple comparisons test (**E**-**H**). See also **Figure S4**.

Figure 5. LDHB promotes V-ATPase-dependent lysosomal acidification in oxidative and glycolytic cancer cells. (**A**) Representative images of a proximity ligation assay of SiHa cells transfected as indicated. LDHB-V-ATPase A1 protein-protein interactions appear as red dots and F-actin is stained in green with phalloidin-FITC. The graph shows mean number of interactions per cell (scale bar 20 μm, n = 3). (**B**) Co-immunoprecipitation of LDHB with V-ATPase A1 subunit in SiHa cells (representative of n = 3). (**C**) SiHa cells transfected with an empty vector or with a plasmid encoding full-length LDHB. Lysosomal pH was assayed 48 hr later in cells treated overnight with or without 100 nM bafilomycin A1 (n = 4). (**D**) Mature and immature lysosomal cysteine cathepsins B detected by immunoblotting in SiHa cells transfected as indicated (n = 5). (**E-G**) Cell count (n = 3) (E),

cell content in acidic vesicles measured using acridine orange staining (n = 3) (F), and cell count after a treatment with or without 20 μM chloroquine for 48 hr (n = 6) (G) of SiHa-ρ0 cells. (**H**) Model describing the contribution of LDHB to lysosomal activity in a metabolic symbiosis based on lactate exchange between glycolytic and oxidative cancer cells. (**I**) Mice were implanted with HCT116 cancer cells carrying shCTR, shLDHB-1 or shLDHB-3, and 2 mg/ml doxycycline was administered via the drinking water 13 days after tumor inoculation. Where indicated, 25 mg/kg chloroquine was administered by intraperitoneal injection every 3 days. Each mouse was bearing a shCTR and a shLDHB tumor, and experiments were run simultaneously. The graph depicts tumor growth normalized to tumor size at treatment initiation (n = 6-14 mice per group). (**J, K**) Western blot analysis of LDHB expression and immunohistochemical detection of ATG12 expression in shLDHB-1 and matched shCTR (I, n = 8) or shLDHB-3 and matched shCTR (K, n = 6) tumors at the end of the experiment shown in (I). (**L, M**) Western blot (L) and immunohistochemistry (M) analysis of LC3-I and LC3-II in the shLDHB-1 and matched shCTR tumors at the end of the experiment shown in (I) (n = 8, scale bar 20 μm). All data represent means ± SEM. *$p < 0.05$, **$p < 0.01$, ***$p < 0.005$, ns, not significant, by two-tailed unpaired Student's t test (**A**, **D**, **E**, **L**, **M**), Mann Whitney test (**F**), one-way ANOVA with Holm-Sidak's multiple comparisons test (**C**, **G, J, K**). See also **Figure S5**.

Figure 1

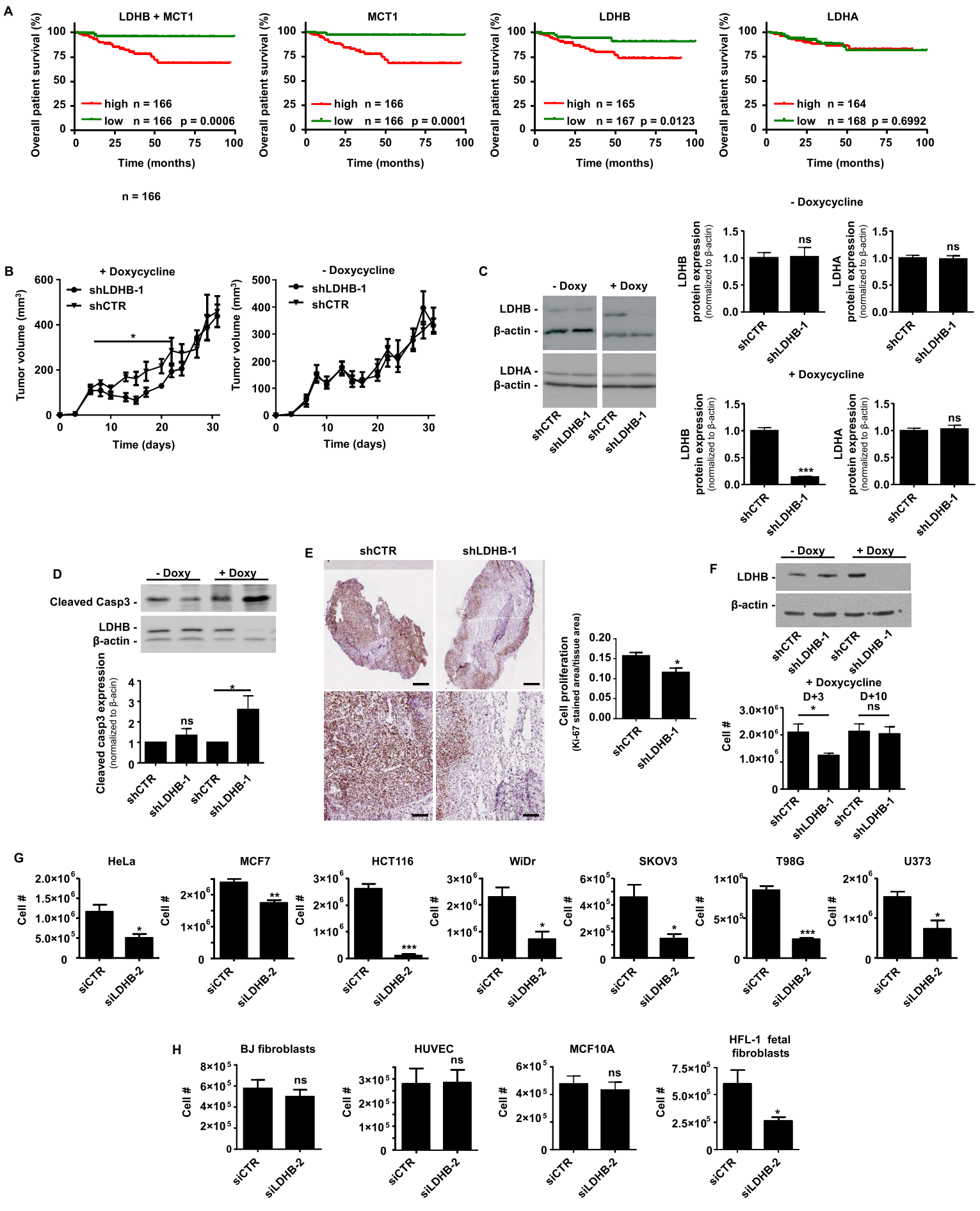
Figure 1
A
LDHB + MCT1
MCT1
LDHB
LDHA
Overall patient survival (%)
Time (months)
high n = 166
low n = 166 p = 0.0006
high n = 166
low n = 166 p = 0.0001
high n = 165
low n = 167 p = 0.0123
high n = 164
low n = 168 p = 0.6992
n = 166
B
+ Doxycycline
- Doxycycline
shLDHB-1
shCTR
Tumor volume (mm3)
Time (days)
C
- Doxy
+ Doxy
LDHB -
β-actin -
LDHA -
shCTR
shLDHB-1
- Doxycycline
+ Doxycycline
LDHB protein expression (normalized to β-actin)
LDHA protein expression (normalized to β-actin)
ns
D
Cleaved Casp3 -
Cleaved casp3 expression (normalized to β-acin)
E
shCTR
shLDHB-1
Cell proliferation (Ki-67 stained area/tissue area)
F
Cell #
D+3
D+10
G
HeLa
MCF7
HCT116
WiDr
SKOV3
T98G
U373
siCTR
siLDHB-2
H
BJ fibroblasts
HUVEC
MCF10A
HFL-1 fetal fibroblasts

Figure 2

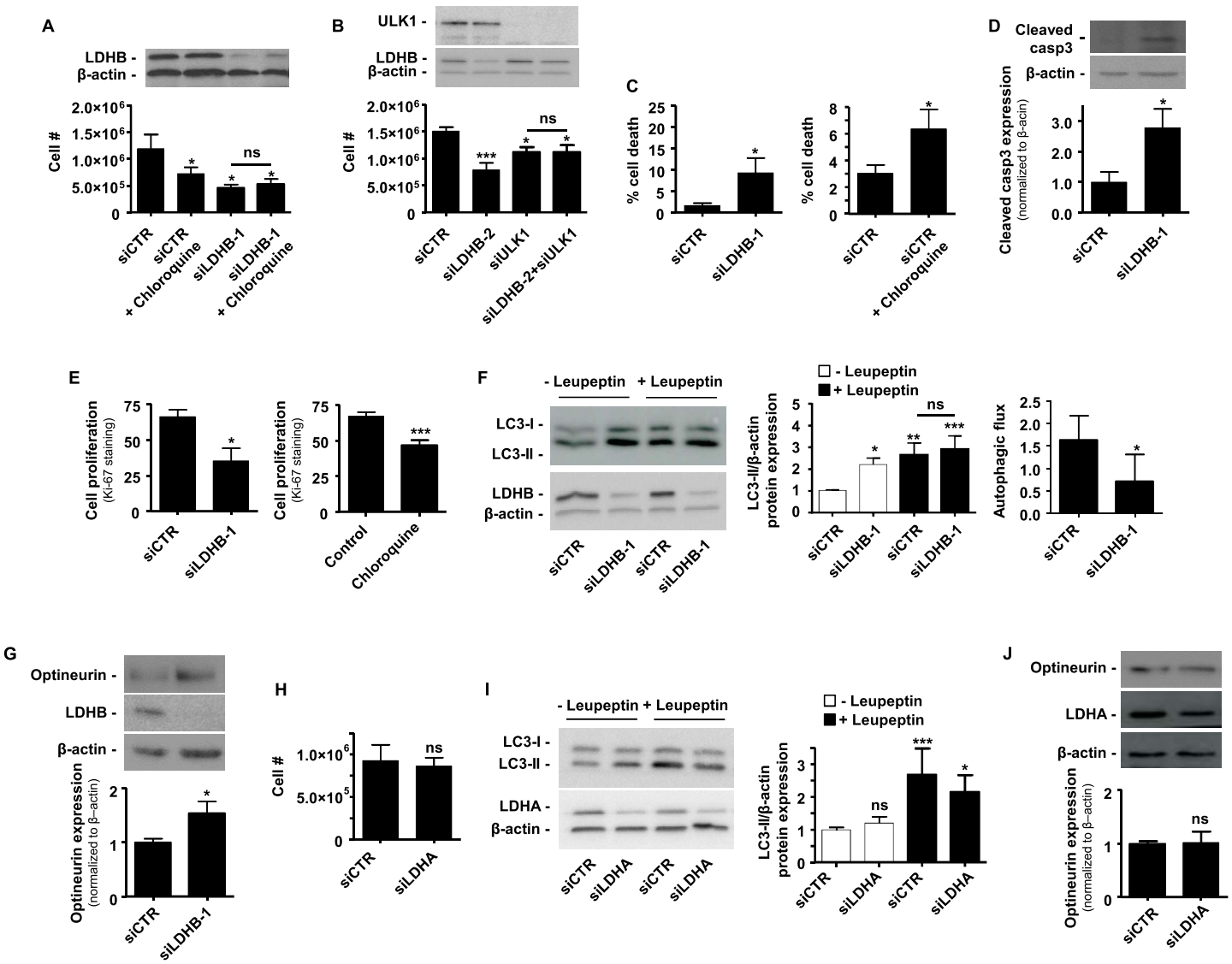
Figure 2
A
LDHB -
β-actin -
Cell #
2.0×10^6
1.5×10^6
1.0×10^6
5.0×10^5
0
ns
siCTR
siCTR + Chloroquine
siLDHB-1
siLDHB-1 + Chloroquine
B
ULK1 -
LDHB -
β-actin -
Cell #
ns
siCTR
siLDHB-2
siULK1
siLDHB-2+siULK1
C
% cell death
siCTR
siLDHB-1
% cell death
siCTR
siCTR + Chloroquine
D
Cleaved casp3 -
β-actin -
Cleaved casp3 expression (normalized to β-actin)
siCTR
siLDHB-1
E
Cell proliferation (Ki-67 staining)
siCTR
siLDHB-1
Cell proliferation (Ki-67 staining)
Control
Chloroquine
F
- Leupeptin
+ Leupeptin
LC3-I -
LC3-II -
LDHB -
β-actin -
siCTR
siLDHB-1
siCTR
siLDHB-1
- Leupeptin
+ Leupeptin
LC3-II/β-actin protein expression
ns
siCTR
siLDHB-1
siCTR
siLDHB-1
Autophagic flux
siCTR
siLDHB-1
G
Optineurin -
LDHB -
β-actin -
Optineurin expression (normalized to β-actin)
siCTR
siLDHB-1
H
Cell #
ns
siCTR
siLDHA
I
- Leupeptin
+ Leupeptin
LC3-I -
LC3-II -
LDHA -
β-actin -
siCTR
siLDHA
siCTR
siLDHA
- Leupeptin
+ Leupeptin
LC3-II/β-actin protein expression
ns
siCTR
siLDHA
siCTR
siLDHA
J
Optineurin -
LDHA -
β-actin -
Optineurin expression (normalized to β-actin)
ns
siCTR
siLDHA

Figure 3

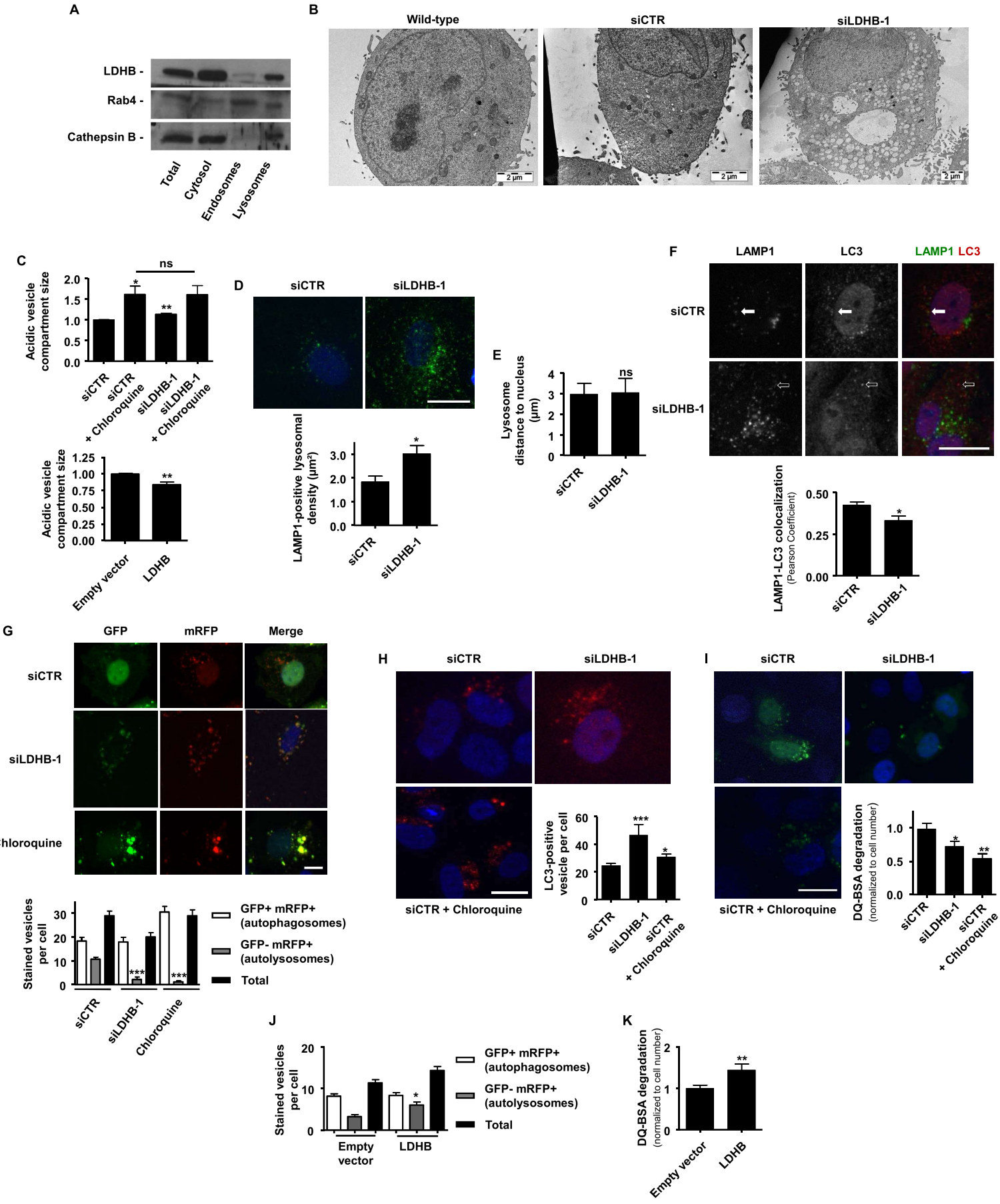
A
LDHB -
Rab4 -
Cathepsin B -
Total
Cytosol
Endosomes
Lysosomes
B
Wild-type
siCTR
siLDHB-1
2 µm
C
Acidic vesicle compartment size
ns
siCTR
siCTR + Chloroquine
siLDHB-1
siLDHB-1 + Chloroquine
Empty vector
LDHB
D
siCTR
siLDHB-1
LAMP1-positive lysosomal density (µm²)
E
Lysosome distance to nucleus (µm)
F
LAMP1
LC3
LAMP1 LC3
LAMP1-LC3 colocalization (Pearson Coefficient)
G
GFP
mRFP
Merge
Chloroquine
Stained vesicles per cell
GFP+ mRFP+ (autophagosomes)
GFP- mRFP+ (autolysosomes)
Total
H
siCTR + Chloroquine
LC3-positive vesicle per cell
I
DQ-BSA degradation (normalized to cell number)
J
K

Figure 4

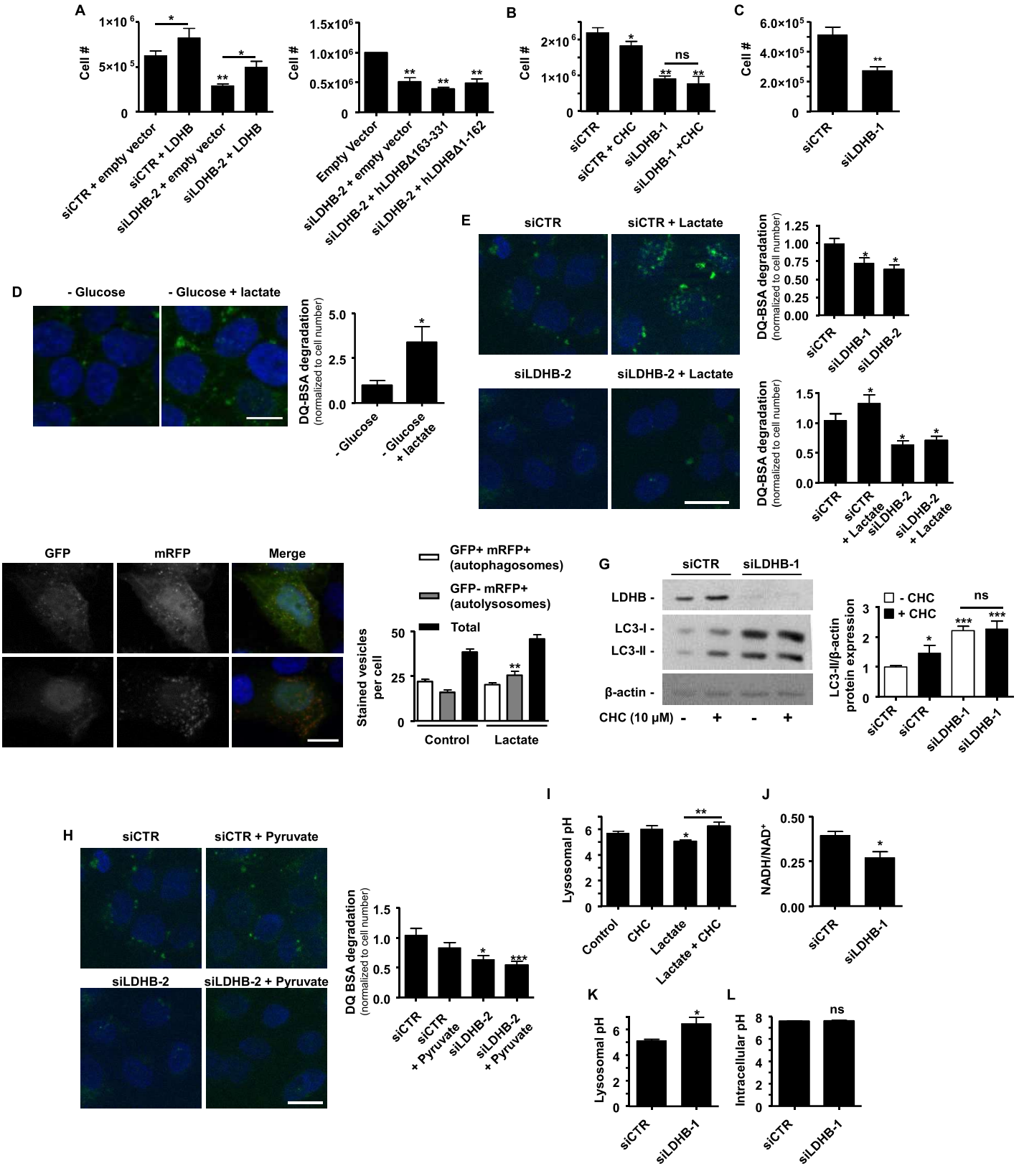
A
Cell #
siCTR + empty vector
siCTR + LDHB
siLDHB-2 + empty vector
siLDHB-2 + LDHB
Empty Vector
siLDHB-2 + empty vector
siLDHB-2 + hLDHBΔ163-331
siLDHB-2 + hLDHBΔ1-162
B
siCTR
siCTR + CHC
siLDHB-1
siLDHB-1 +CHC
ns
C
siCTR
siLDHB-1
D
- Glucose
- Glucose + lactate
DQ-BSA degradation
(normalized to cell number)
- Glucose
- Glucose + lactate
E
siCTR
siCTR + Lactate
siLDHB-2
siLDHB-2 + Lactate
DQ-BSA degradation
(normalized to cell number)
siCTR
siLDHB-1
siLDHB-2
siCTR + Lactate
siLDHB-2 + Lactate
F
GFP
mRFP
Merge
Control
Lactate
GFP+ mRFP+ (autophagosomes)
GFP- mRFP+ (autolysosomes)
Total
Stained vesicles per cell
Control
Lactate
G
siCTR
siLDHB-1
LDHB -
LC3-I -
LC3-II -
β-actin -
CHC (10 μM) - + - +
- CHC
+ CHC
ns
LC3-II/β-actin protein expression
siCTR
siCTR
siLDHB-1
siLDHB-1
H
siCTR
siCTR + Pyruvate
siLDHB-2
siLDHB-2 + Pyruvate
DQ BSA degradation
(normalized to cell number)
siCTR
siCTR + Pyruvate
siLDHB-2
siLDHB-2 + Pyruvate
I
Lysosomal pH
Control
CHC
Lactate
Lactate + CHC
J
NADH/NAD+
siCTR
siLDHB-1
K
Lysosomal pH
siCTR
siLDHB-1
L
Intracellular pH
ns
siCTR
siLDHB-1

Figure 5

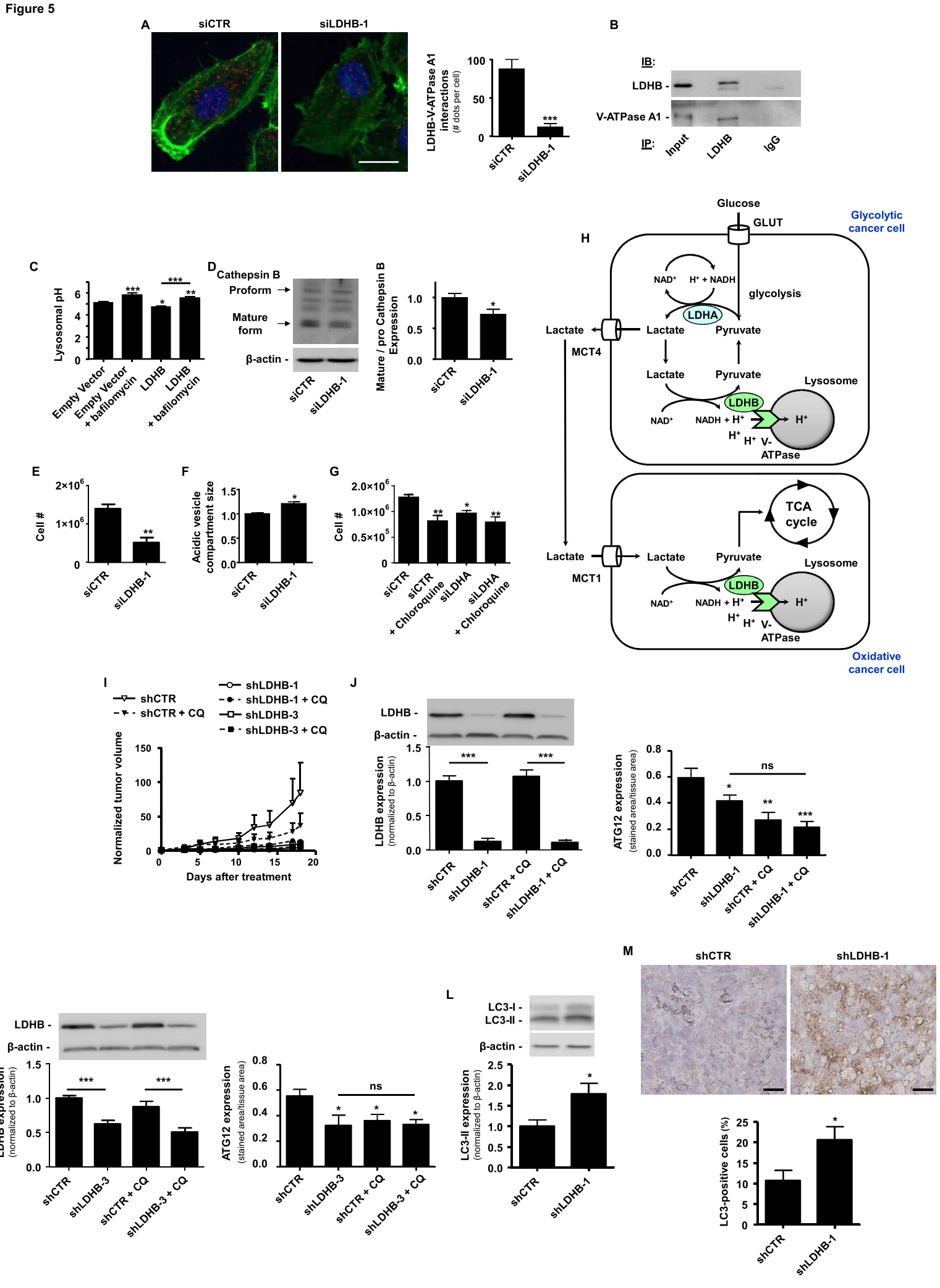
Figure 5
A
siCTR
siLDHB-1
LDHB-V-ATPase A1 interactions (# dots per cell)
B
IB:
LDHB -
V-ATPase A1 -
IP:
Input
LDHB
IgG
C
Lysosomal pH
Empty Vector
Empty Vector + bafilomycin
LDHB
LDHB + bafilomycin
D
Cathepsin B
Proform
Mature form
β-actin -
Mature / pro Cathepsin B Expression
E
Cell #
F
Acidic vesicle compartment size
G
Cell #
siCTR
siCTR + Chloroquine
siLDHA
siLDHA + Chloroquine
H
Glucose
GLUT
Glycolytic cancer cell
glycolysis
LDHA
Lactate
Pyruvate
MCT4
MCT1
Lysosome
LDHB
V-ATPase
TCA cycle
Oxidative cancer cell
I
shCTR
shCTR + CQ
shLDHB-1
shLDHB-1 + CQ
shLDHB-3
shLDHB-3 + CQ
Normalized tumor volume
Days after treatment
J
LDHB -
β-actin -
LDHB expression (normalized to β-actin)
ATG12 expression (stained area/tissue area)
ns
K
LDHB -
β-actin -
LDHB expression (normalized to β-actin)
ATG12 expression (stained area/tissue area)
L
LC3-I -
LC3-II -
β-actin -
LC3-II expression (normalized to β-actin)
M
shCTR
shLDHB-1
LC3-positive cells (%)

SUPPLEMENTAL DATA

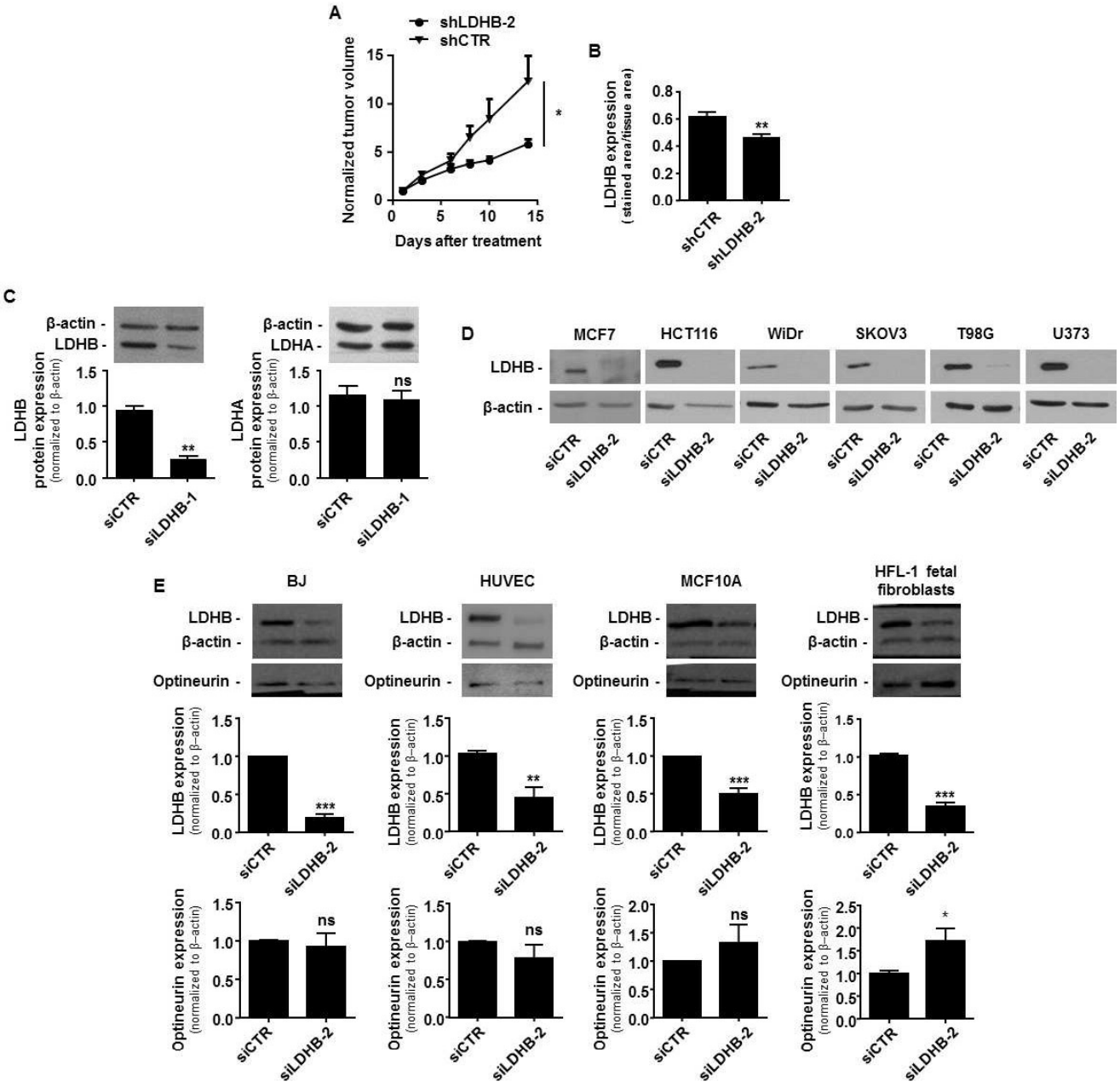

Figure S1. Silencing LDHB preferentially inhibits autophagy in cancer cells (related to Figure 1). (**A**) Mice were implanted with HCT116 cancer cells carrying shCTR or shLDHB-2 and doxycycline (2 mg/ml) was administered via the drinking water 12 days after tumor inoculation. The graph depicts tumor growth (n = 8 mice per group). (**B**) Immunohistochemical detection of LDHB expression in tumors collected in the animals treated with doxycycline at the end of the experiment shown in (A) (n = 8). (**C**) Representative western blots and quantification of LDHB and LDHA at 72 hr in HeLa cells transfected as indicated (n = 6). (**D**) Representative western blots (n = 3-4) of LDHB expression in different types of human cancer cells transfected as indicated. (**E**) Representative western blots and quantification of LDHB and optineurin in 4 nonmalignant cell lines transfected as indicated (n = 4-6). All data represent means ± SEM. *p < 0.05, **p < 0.01, ***p < 0.005, ns, not significant, by two-way ANOVA (**A**), two-tailed unpaired Student's t test (**B**), or Mann Whitney test (**C, E**).

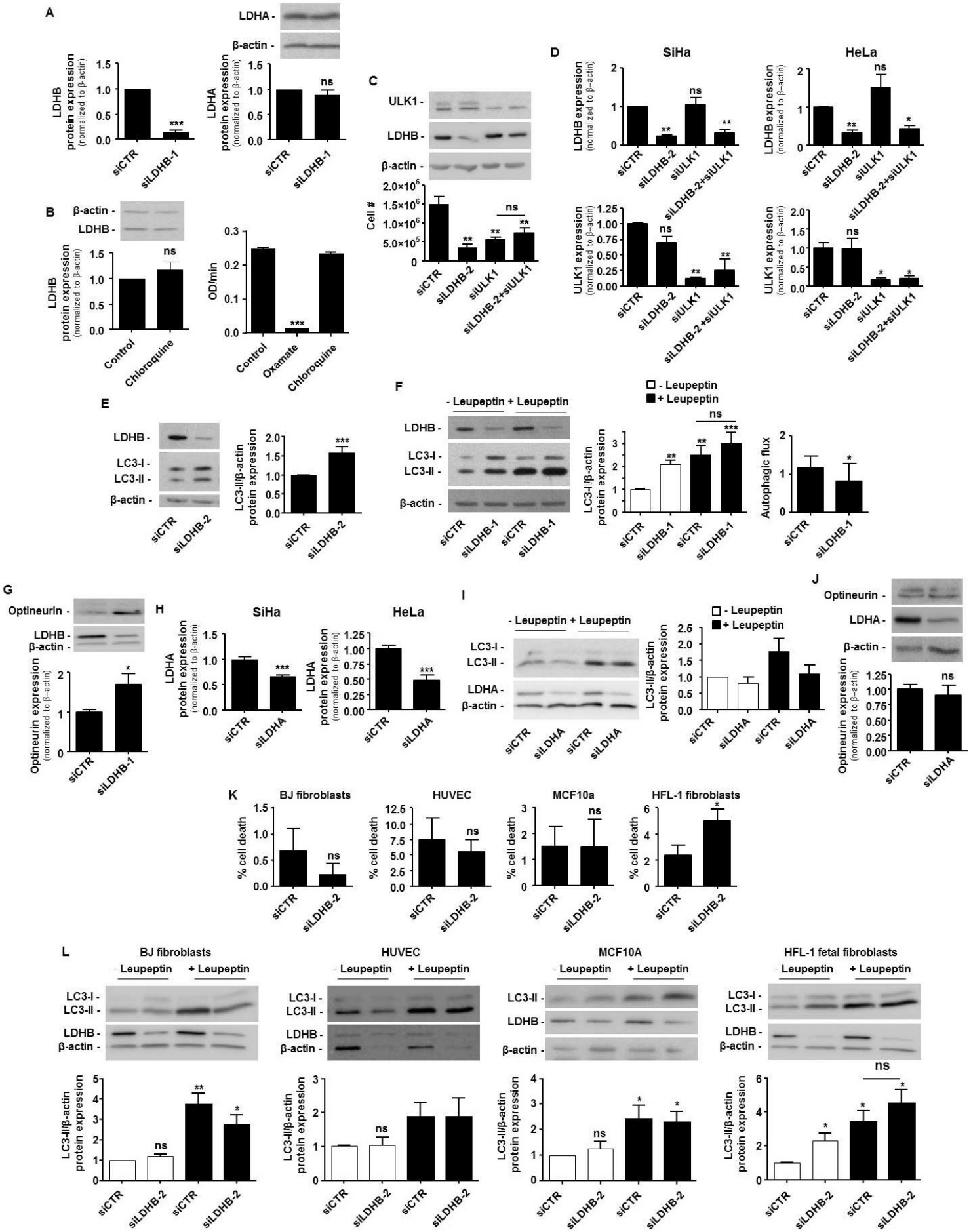
A
LDHB protein expression (normalized to β-actin)
siCTR
siLDHB-1
LDHA -
β-actin -
LDHA protein expression (normalized to β-actin)
ns
B
β-actin -
LDHB -
LDHB protein expression (normalized to β-actin)
Control
Chloroquine
OD/min
Oxamate
C
ULK1 -
LDHB -
β-actin -
Cell #
siULK1
siLDHB-2+siULK1
D
SiHa
HeLa
LDHB expression (normalized to β-actin)
ULK1 expression (normalized to β-actin)
E
LC3-I -
LC3-II -
LC3-II/β-actin protein expression
F
- Leupeptin + Leupeptin
Autophagic flux
G
Optineurin -
Optineurin expression (normalized to β-actin)
H
LDHA protein expression (normalized to β-actin)
siLDHA
I
J
K
BJ fibroblasts
HUVEC
MCF10a
HFL-1 fibroblasts
% cell death
L
MCF10A
HFL-1 fetal fibroblasts

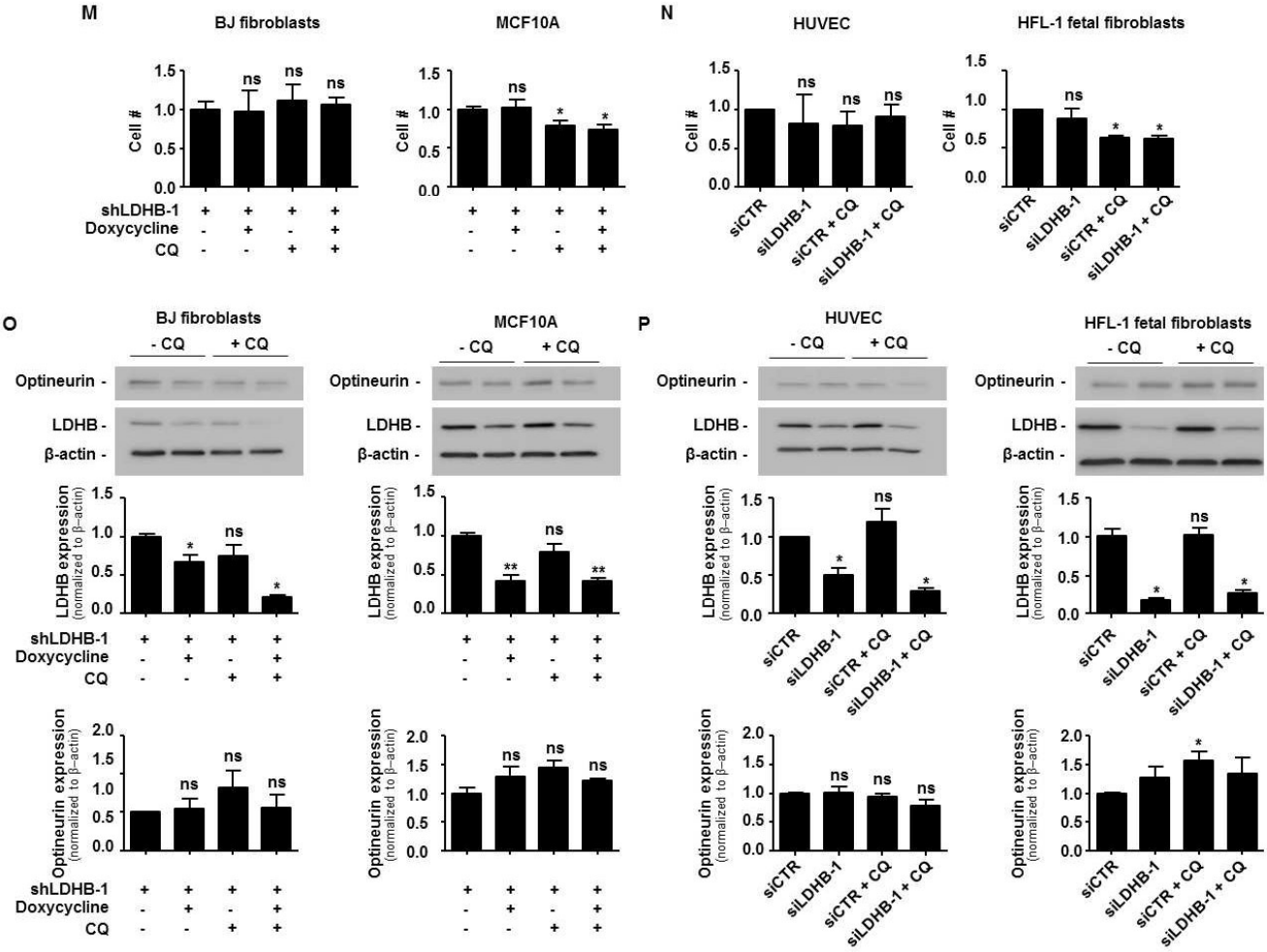

Figure S2. LDHB promotes basal autophagy flux preferentially in oxidative cancer cells (related to Figure 2). (**A**) Quantification of LDHB (n = 13) and LDHA (n = 6) protein expression in SiHa cells carrying siCTR or siLDHB-1. Representative western blots are shown for LDHA and in **Figure 2F** for LDHB. (**B**) LDHB expression in SiHa cells treated for 48 hr with or without 20 μM chloroquine (n = 6) and catalytic activity of LDHB in the lysates of SiHa cell treated for 48 hr and throughout the assay with or without 10 mM oxamate or with or without 20 μM chloroquine (n = 3). (**C**) Numbers of HeLa cells and representative western blot of ULK1 and LDHB expression 72 hr after transfection as indicated (n = 6). (**D**) Quantification of LDHB and ULK1 protein expression in SiHa and HeLa cells transfected as indicated (n = 6). (**E**) Representative western blots and quantification of LC3-I and LC3-II in SiHa cells transfected with siCTR or siLDHB-2 (n = 4). (**F**) Representative western blot and quantification of LC3-II (n = 6) in HeLa cells transfected as indicated and treated overnight with or without 150 μM leupeptin, and autophagic flux calculated as the difference of LC3-II expression between conditions treated with and without leupeptin. (**G**) Representative western blot and quantification of optineurin in HeLa cells transfected with siCTR or siLDHB-1 (n = 6). (**H**) Quantification of LDHA protein expression in SiHa and HeLa cells transfected with siCTR or siLDHA. Representative western blots are show in **Figures 2I** and **S2I**. (**I**) As in (F) but with siLDHA (n = 4). (**J**) Representative western blot and quantification of optineurin in Hela cells transfected with siCTR or siLDHA (n = 4). (**K**) Cell death measured by trypan blue exclusion in nonmalignant cell lines carrying siCTR or siLDHB-2 (n = 4-6). (**L**) As in (F) but with nonmalignant cell lines (n = 4-6). (**M**) Numbers of BJ and MCF10A cells carrying shCTR or shLDHB-1 and treated with or without 1 μg/ml doxycycline and with or without 25 μM chloroquine (CQ) for 72 hr (n = 3-6). (**N**) Number of HUVECs and HFL-1 fibroblasts carrying siCTR or siLDHB-1 and treated for 72 hr with or without 25 μM chloroquine (CQ) (n = 3). (**O**) Representative western blots and quantification of LDHB and optineurin expression in cells treated as in (M) (n = 3-6). (**P**) Representative western blots and quantifications of LDHB and optineurin expression in cells treated as in (N) (n = 3-6). All data represent means ± SEM. *p < 0.05, **p < 0.01, ***p < 0.005, ns, not significant, by Wilcoxon Signed Rank test (**A**, **B**), one-way ANOVA with Holm-Sidak's multiple comparisons test (**B**, **C**), Mann Whitney test (**E**, **F** right, **G**, **H**, **J**), Kruskal-Wallis with Dunn's multiple comparisons test (**D**, **F** middle, **I**), two-tailed unpaired Student's t test (**K**) or one sample t-test (**M**, **N**, **O**, **P**).

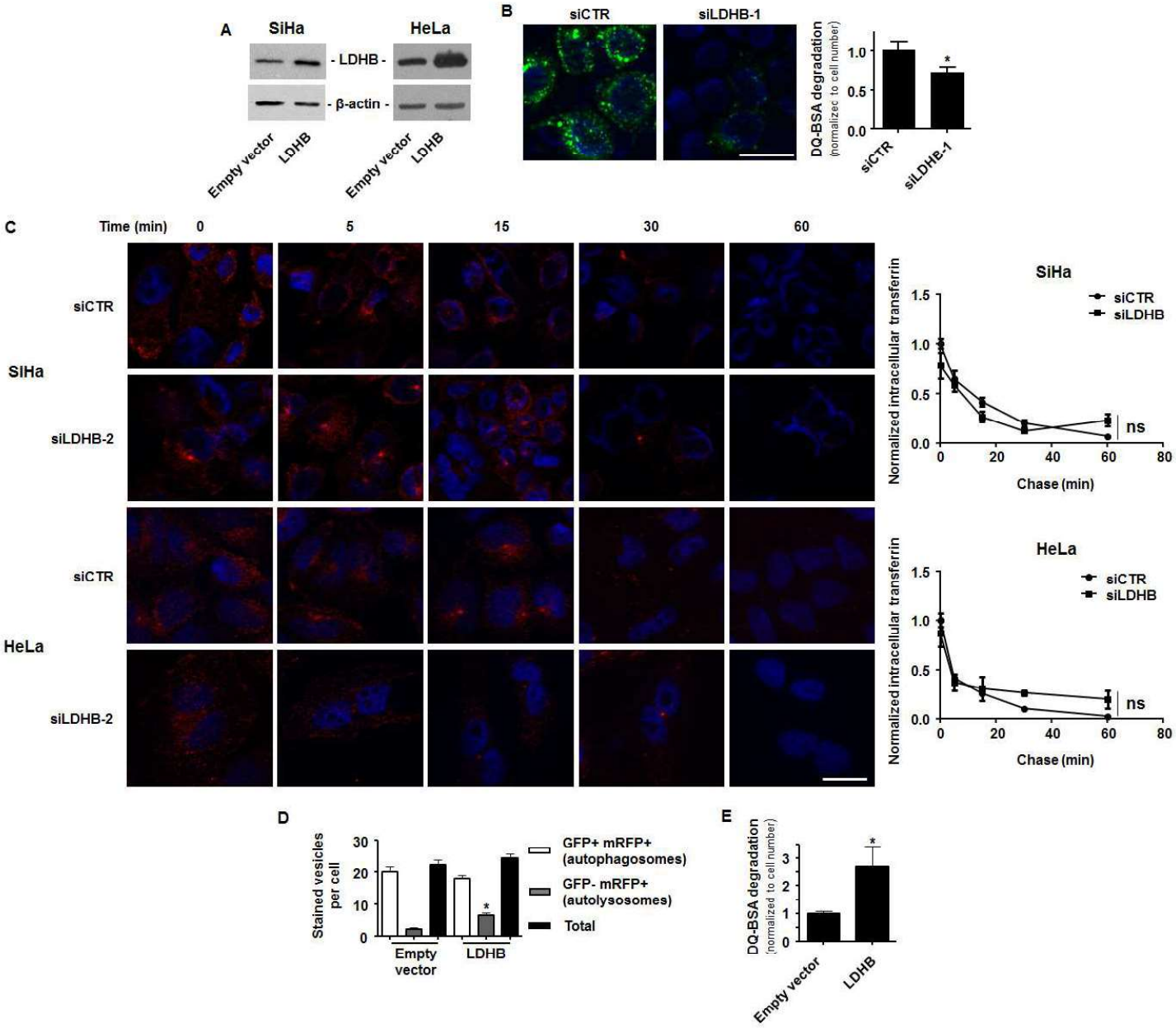

Figure S3. LDHB controls autophagic vesicle maturation but not early endosome trafficking in oxidative cancer cells (related to Figure 3). (**A**) Representative western blots of SiHa and HeLa cells with or without ectopic LDHB overexpression. (**B**) Intracellular proteolytic activity of HeLa cells measured with DQ-BSA dequenching 48 hr after transfection with or without ectopic LDHB overexpression (scale bar 20 µm, n = 4). (**C**) Fluorescent transferrin recycling by SiHa and HeLa cells, where figures show transferrin (red fluorescence) chase over time and the graphs transferrin abundance in cells normalized to time 0 (scale bar 20 µm, n = 3). (**D**) Autophagosome and autolysosome abundance measured with a LC3-GFP-mRFP reporter in HeLa cells transfected with or without ectopic LDHB overexpression (n = 4). (**E**) Quantification of intracellular proteolysis (DQ-BAS assay) in HeLa cells with or without ectopic LDHB overexpression (scale bare 20 µm, n = 4). All data represent means ± SEM. *p < 0.05, **p < 0.01, ***p < 0.005, ns, not significant, by Mann Whitney test (**B**, **E**), two-way ANOVA (**C**) or Kruskal-Wallis with Dunn's multiple comparisons test (**D**).

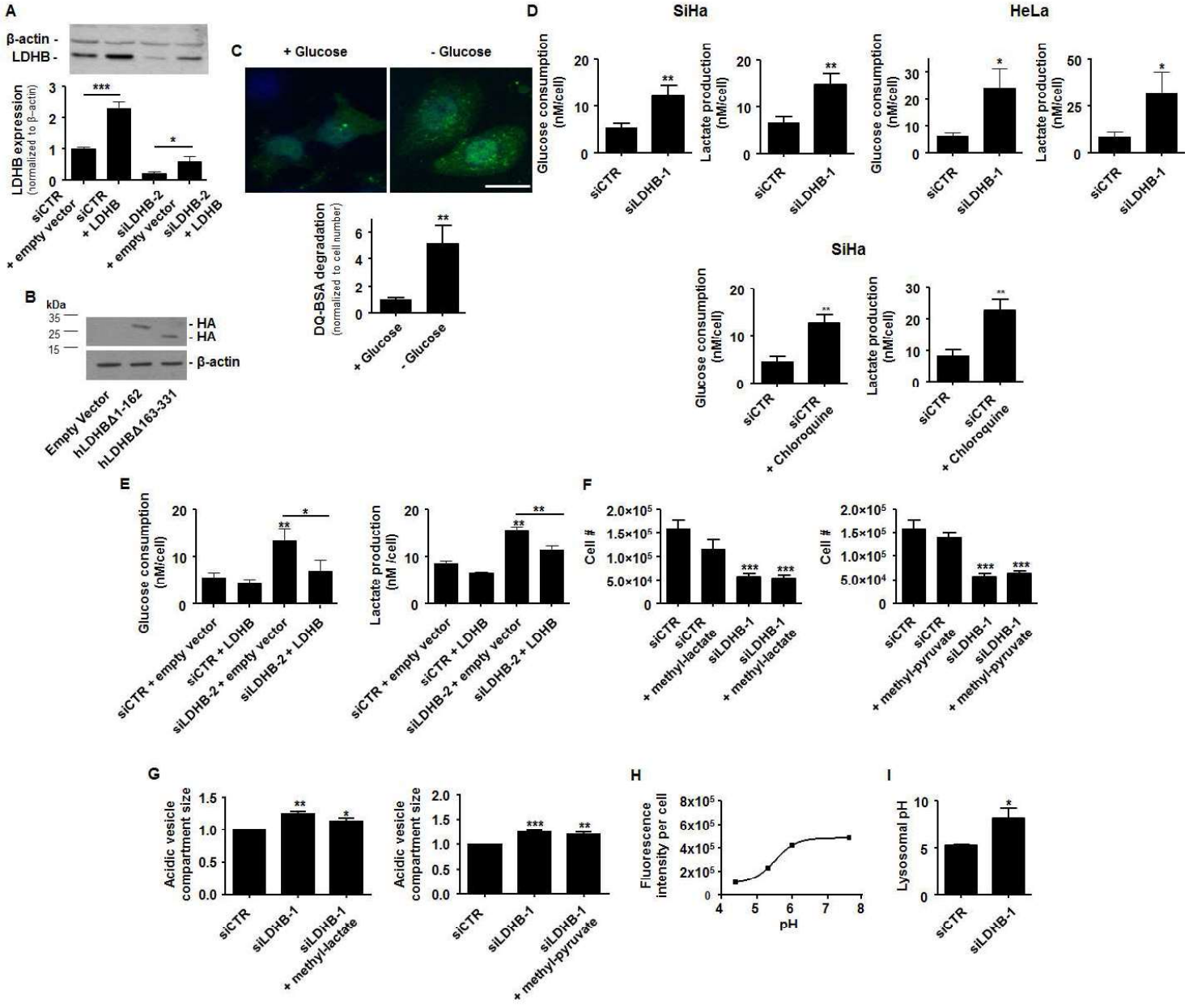

Figure S4. LDHB actively controls lysosomal acidity in oxidative cancer cells (related to Figure 4). (**A**) Representative western blots and quantification of ectopic LDHB re-expression in SiHa cells carrying siCTRor siLDHB-2 (n = 4). (**B**) Representative western blots (n = 3) of the expression of HA-tagged truncated forms of LDHB in siLDHB-2-expressing SiHa cells (scale bar 10 µm). (**C**) Representative images and quantification of intracellular proteolysis in overnight glucose-starved cells using DQ-BSA dequenching (scale bar 20 µm, n = 4). (**D**) Glucose consumption and lactate release over 72 hr by SiHa and HeLa cells treated for 48 hr with or without 20 µM chloroquine (n = 6). (**E**) Glucose consumption and lactate release by SiHa cells transfected as indicated (n = 4). (**F**) Numbers of SiHa cells treated transfected with siCTR or siLDHB-1 and treated for 72 hr with or without 10 mM methyl-pyruvate or with or without 10 mM methyl-lactate (n = 4). (**G**) Content in acidic vesicles measured with acridine orange staining of SiHa cells transfected with siCTR or with siLDHB-1 and treated for 72 hr with or without 10 mM methyl-pyruvate or with or without 10 mM methyl-lactate (n = 4). (**H**) Representative calibration curve of lysosomal pH measurements with FITC-dextran in SiHa cells (n = 3). (**I**) Lysosomal pH measured with FITC-dextran in HeLa cells (n = 3). All data represent means ± SEM. *p < 0.05, **p < 0.01, ***p < 0.005, ns, not significant, by two-tailed unpaired Student's t test (**C, D, I**), one-way ANOVA with Holm-Sidak's (**E**, **F**) or Kruskal-Wallis with Dunn's multiple comparisons test (**G**).

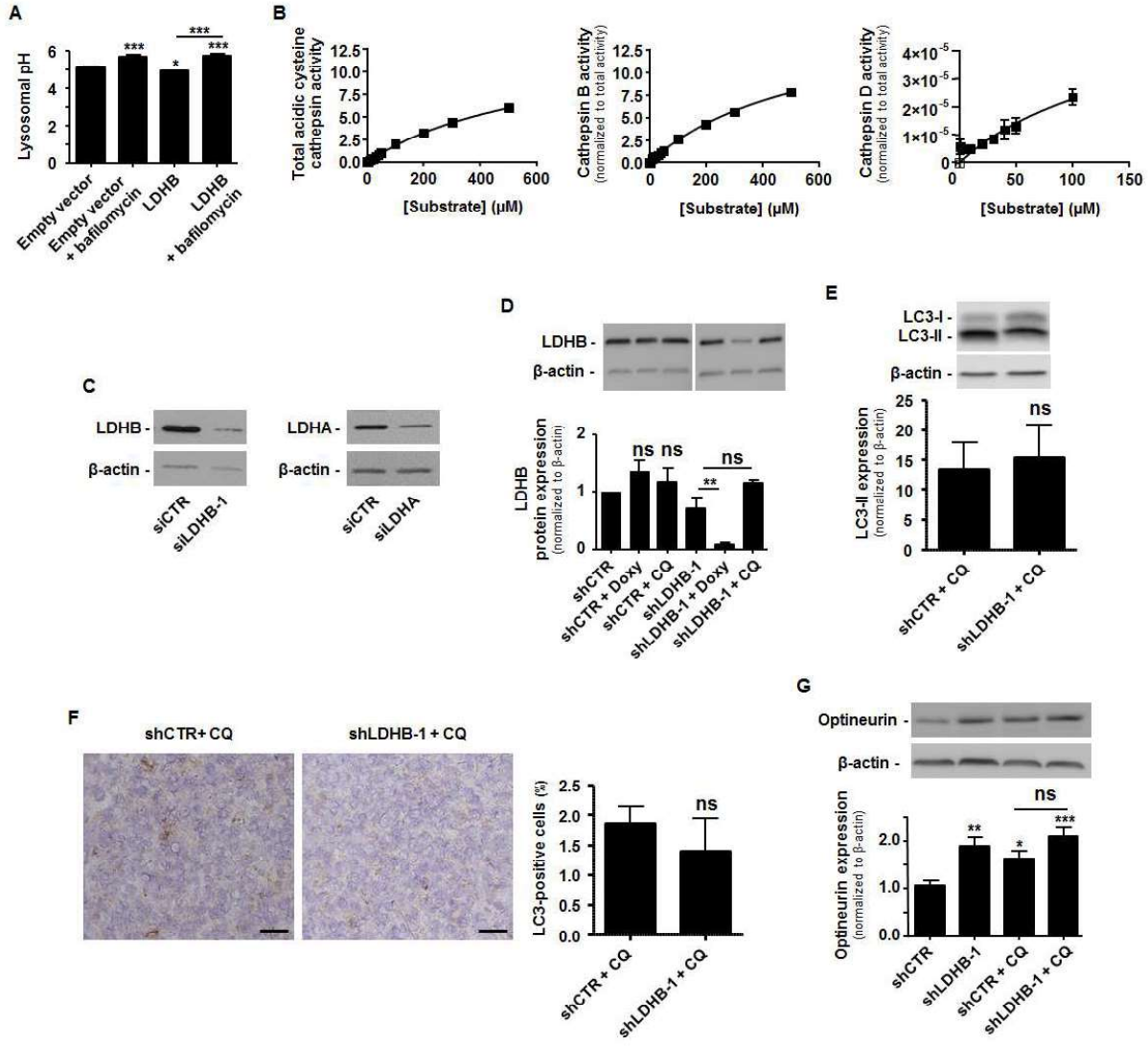

Figure S5. LDHB promotes lysosomal acidification and protease activation in cancer cells (related to Figure 5). (**A**) Lysosomal pH measured with FITC-dextran in HeLa cells with or without ectopic LDHB overexpression treated overnight with or without 100 nM of bafilomycin A1 (n = 4). (**B**) Enzymatic activities of total acidic cysteine cathepsins, cysteine cathepsins B and aspartyl cathepsins D measured using fluorogenic substrates in SiHa cell lysates at pH 5.5 (n = 5). (**C**) Representative western blots (n = 3-4) showing LDHB and LDHA expression in SiHa-ρ0 cells 72 hr after siCTR, siLDHB or siLDHA transfection. (**D**) Representative western blots and quantification of LDHB expression in HCT116 cells expressing shCTR or shLDHB-1 and treated in vitro with or without 2 μg/ml doxycycline (Doxy) and with or without 25 μM chloroquine (CQ) for 48 hr (n = 4). (**E**) Each mouse was implanted with two HCT116 tumors carrying either shCTR or shLDHB-1, and 2 mg/ml doxycycline was administered via the drinking water 13 days after tumor inoculation. Where indicated, 25 mg/kg chloroquine was further administered intraperitoneally every 3 days. (**E, F**) Western blot (E) and immunohistochemistry (F) analysis of LC3-I and LC3-II at the end of the experiment shown in Figure 5I in shLDHB-1 and shCTR tumors from mice that received chloroquine (scale bar 20 μm, n = 8). (**G**) Representative western blot of optineurin expression in tumors collected at the end of the treatment, in the same gel as in Figure 5J (same β-actin control; n = 8). All data represent means ± SEM. *p < 0.05, **p < 0.01, ***p < 0.005, ns, not significant, by one-way ANOVA with Holm-Sidak's test (**A, D, G**) or two-tailed unpaired Student's t test (**E**, **F**).

SUPPLEMENTAL EXPERIMENTAL PROCEDURES

In vivo experiments

Anesthetized (ketamine/xylazine) 8 weeks-old male BALB/c nude mice (Elevage Janvier) received bilateral subcutaneous injections of 10^6 SiHa cancer cells in 300-µl of growth factor-reduced Matrigel. One day after tumor implantation, mice were randomly assigned to a treatment group receiving 3 % sucrose with or without 1 mg/ml doxycycline in the drinking water. Animals were sacrificed 30 days after tumor implantation, and tumors were snap-frozen in liquid nitrogen-cooled isopentane for further protein expression and immunohistochemical analyses. Tumor generation with HCT116 cells expressing shCTR, shLDHB-1, shLDHB-2 or shLDHB-3 were conducted as described for SiHa cells, except that $2x10^6$ cells were injected in 100 µl of saline solution, doxycycline (2 mg/ml) was administered 12-13 days after tumor implantation (when tumor reached ~5 mm diameter), and animals were sacrificed after 15 (shLDHB-2) to 18 (shLDHB-1 and shLDHB-3) days on doxycycline. Mice were treated with intraperitoneal injection of chloroquine at 25 mg/kg every 3 days (Lakhter et al., 2013).

Cell culture

SiHa and HeLa human cervix carcinoma cells (ATCC), MCF7 human breast cancer cells (ATCC), HCT116 and WiDr human colon carcinoma cells (ATCC), SKOV3 human ovarian carcinoma cells (Wintzell et al., 2012), T98G and U373 human glioblastoma cells (Bruyere et al., 2011), and BJ normal human skin fibroblasts (ATCC) were routinely cultured in DMEM with 4.5 g/l glucose, 4 mM glutamine and 10 % FCS (full DMEM) at 37 °C in a humidified 5 % CO_2 incubator. HFL-1 fetal human lung fibroblasts (ATCC, (Breul et al., 1980)) were routinely cultured in F12-K medium supplemented with 10 % FCS, human umbilical vein endothelial cells (HUVEC, Sigma-Aldrich) in ECGM (Sigma-Aldrich), and MCF10A normal human mammary gland epithelial cells in DMEM:F-12 with 5 % horse serum, 1 mM $CaCl_2$, 10 mM Hepes, 10 µg/ml insulin, 20 ng/ml EGF and 0.5 µg/ml hydrocortisone. Mitochondria-defective SiHa-ρ0 cells were generated by treating wild-type SiHa cells with low-dose ethidium bromide (50 ng/ml) for 7 weeks, as previously described and characterized (Sonveaux et al., 2008; Porporato et al., 2014). SiHa-ρ0 cells were routinely grown in full DMEM added with 1 mM pyruvate and 50 ng/ml uridine. Assay media were either full DMEM or glucose-deprived DMEM (D5030, Sigma-Aldrich) reconstituted without glucose, glutamine and serum. For the assessment of cell survival under glucose starvation, cells were harvested 48 hr post-siRNA transfection and plated at an equal density to avoid bias due to unequal proliferation rates. Glucose starvation was performed during 6 hr after cell adhesion.

RNA interference and cell transfection

TRIPZ-inducible lentiviral vector expression control shRNA (shCTR) and human LDHB shRNA (shLDHB-1: TTAACATTTCTCTGCACCA, shLDHB-2: TATTGTTTGGAACTGTTGC, shLDHB-3: AAGGTAGCGAAATCTAGCA, RHS5087-EG3945, Dharmacon) were used for lentivirus preparation (trans-lentiviral packaging mix, Dharmacon) and stable SiHa, HCT116, BJ and MCF10A cell infection. Selection was performed with puromycin (1 µg/ml) and lentiviral expression was induced with doxycycline (0.5 to 2 µg/ml).

siRNAs were transfected with lipofectamine RNAiMAX (Invitrogen) in Opti-MEM according to manufacturer's recommendations. siLDHB-1 targeted 5' AAG AUU GUA GUG GUA ACU GCA-3'; siLDHB-2 5' GCA GCU GAC UUU GUC UUC U-3' at the 5'UTR of LDHB mRNA; siLDHA 5'-GGC AAA GAC UAU AAU GUA A-3'; and siULK1 was a SMARTpool ON-TARGETplus ULK1 siRNA. Allstars/siCTR (Qiagen) were used as negative controls.

Plasmids were transfected with TransIT-2020 (Mirus) in Opti-MEM according to manufacturer's recommendations. Reexpression transfections were performed 24 hr after transfection with siCTR or siLDHB-2. All measurements were performed 48 hr and 72 hr after plasmid and siRNA transfection, respectively.

For the production of HA-tagged LDHB constructs, human LDHB cDNA was initially purchased from Origene (Cat. No SC319772, Ref. ID NM_002300). For the construction of HA-tagged 1004 ORF of hLDHB (fl [full-length] hLDHB), hLDHBΔ163-331 and hLDHBΔ1-162, cDNA-specific oligonucleotides upstream and downstream of the hLDHB ORF respectively containing EcoRI and NotI sites were used to generate polymerase chain reaction fragments. These fragments were cloned into a pcDNA3HA vector and sequenced at Macrogen using T7 and SP6 promoter primers. Primers were: full-length hLDHB, 5'-CAT TCC GAA TTC ATG GCA ACT CTT AAG GAA AAA CTC ATT-3' and 5'-AAT GCGGCCGC TCA CAG GTC TTT TAG GTC CTT CTG -3'; hLDHBΔ163-331, 5'-CAT TCC GAA TTC ATG GCA ACT CTT AAG GAA AAA CTC ATT-3'and 5'-AAT GCGGCCGC TCA ACT TCC AAT CAC GCG GTG TTT-3'; hLDHBΔ1-162, 5'-CAT TCC GAA TTC ATG GGA TGT AAT CTG GAT TCT GCT AGA-3' and 5'-AAT GCGGCCGC TCA CAG GTC TTT TAG GTC CTT CTG -3'.

Co-immunoprecipitation

Cells were washed in PBS and scraped on ice in a lysis buffer (2 ml / 75 cm² flask) containing 20 mM HEPES, 100 mM NaCl, 1 mM EDTA, 1% Triton X-100, protease inhibitor cocktail (Sigma) and PhosSTOP Phosphatase Inhibitor Cocktail (Roche), pH 7.4. Immunoprecipitation was performed using Dynabeads protein G (Invitrogen) according to manufacturer's protocol. Briefly 500 µl of cell lysate were incubated for 2 hr at 4°C under agitation with magnetic beads coupled to 3 µg of either mouse monoclonal against LDHB (2H6, Novus Biologicals) or normal mouse control IgG (Dako). After 4 washes with

lysis buffer, immunoprecipitated proteins were eluted with elution buffer provided by the manufacturer and processed for western blotting.

Western blotting

Tissue samples were homogenized in RIPA buffer (50 mM Tris pH 7.4, 150 mM NaCl, 1 % Triton-X-100, 0.05 % sodium deoxycholate, 1 mM EDTA, 0.1 % SDS, protease inhibitor cocktail [Sigma] and PhosSTOP Phosphatase Inhibitor Cocktail [Roche]) using a pellet mixer (VWR) and centrifuged at 12,500 g for 15 min at 4°C to remove debris. Cells were washed with PBS, lysed in RIPA buffer and centrifuged at 10 000 g for 10 minutes to remove cell debris. Immunoblotting was performed as previously described (Feron et al., 1996). Primary antibodies were: a rabbit monoclonal against LDHB (EP1565Y, Novus Biologicals); mouse monoclonals against HA (H9658, Sigma) or β-actin (A5441, Sigma); rabbit polyclonals against LC3B (NB600-1384, Novus Biologicals), cysteine cathepsins B (20-CR71, Fitzgerald), cleaved caspase-3 (Asp175, 9661, Cell signaling), optineurin (ab23666, Abcam or Atlas Antibodies), ULK1 (ab23666, Cell signalling) or Rab4 (ab13252, Abcam); and a sheep polyclonal against lactate dehydrogenase isoenzyme V (ab9002, Abcam). LC3II detection to monitor autophagy was used according to reference (Mizushima and Yoshimori, 2007). Chemiluminescence was detected with an Amersham 600 imager (Amersham, GE Healthcare lifescience). Densitometric analysis was performed with the ImageJ software 1.46r (NIH). Autophagic flux was calculated as the difference of the LC3II protein content with and without the lysosomal protease inhibitor leupeptin.

Immunochemistry and proximity ligation assay

For immunohistochemistry, 5 µm-thick sections were cryosliced. After endogenous peroxidase inhibition for 20 min with 3% H_2O_2 in methanol, slices were blocked, incubated with rabbit anti-Ki67 antibody (clone SP6, Abcam #16667), mouse anti-LC3 monoclonal antibody (clone 5F10, nanoTools), rabbit anti-ATG12 (EPR4800 Novus Biologicals) or rabbit anti-LDHB antibody (Novus Biologicals #EP1565Y) and revealed with HRP-conjugated anti-rabbit antibodies (Jackson Immunoresearch) followed by DAB (Dako). After counterstaining with hematoxylin (Dako), slices were dehydrated and mounted with a Dako coverslipper. Stained slices were then digitalized using a SCN400 slide scanner (Leica) at a 20x magnification. Whole tumor sections were analyzed using TissueIA (Leica). Color deconvolution was applied using hematoxylin and DAB matrices. Thresholds, manually adjusted on representative positive versus negative tissue areas, were applied for tissue and for DAB detection (Bouzin et al., 2016). Results are expressed as stained area/tissue area. Parameters were kept constant for all slices and analysis was performed at 20x magnification.

Immunocytofluorescence labeling was performed as previously described (Sonveaux et al., 2008). Briefly, cells were fixed with a 4 % formaldehyde solution and washed with PBS containing 50 mM NH_4Cl. They were permeabilized with 0.3 % Triton X-100 and blocked with 5 % BSA. DAPI was used to stain cell nuclei.

In situ protein-protein interactions were detected using the proximity ligation assay (PLA, Duolink kit) of Olink Bioscience according to the manufacturer's instructions. This assay detects interactions using a pair of secondary antibodies coupled to positive (probe PLUS) or negative (probe MINUS) complementary DNA strands. DNA-coupled antibody binding is followed by *in situ* DNA hybridization, amplification and detection steps with a fluorescently labeled probe (Duolink detection kit 563). F-actin was stained with phalloidin fluorescein isothiocyanate (phalloidin-FITC) (Sigma). All images were acquired on a Zeiss AxioImager.z1 equipped with an ApoTome module for structured illumination microscopy using the Axiovision software (Zeiss). The relative number of interactions per cell was determined with the BlobFinder image analysis software (Centre for Image Analysis) on a minimum of 100 cells per condition. Primary antibodies were: mouse monoclonals against LDHB (2H6, Novus Biologicals) and LAMP1 (ab25630, Abcam); and a rabbit polyclonal against the A1 subunit of V-ATPase (H140, Santa Cruz).

Cell fractionation

Cells fractionation was performed according to (Schroter et al., 1999). Briefly, 10^8 cells in PBS (total fraction) were homogenized in fractionation buffer (10 mM Tris, 250 mM sucrose, pH 7.0 adjusted with acetic acid) and centrifuged at 2000 g for 2 minutes to remove cellular debris. Supernatant was centrifuged at 4000 g for 2 minutes to pellet plasma membranes and nuclei, which were discarded. Ultracentrifugation of the supernatant at 100,000 g for 2 minutes allowed to pellet mitochondria, endosomes and lysosomes, whereas the resulting concentrated supernatant corresponded to the cytosolic fraction. Pellets were resuspended in 50 µl of bidistillated water in order to destroy lysosomes by osmotic shock for 5 minutes. After centrifugation at 100,000 g for 2 minutes, lysosomal fractions (supernatant) and mitochondrial + endosomal fractions (pellet) were harvested. Proteins were solubilized with Laemmli buffer for the supernatants and with Triton-based lysis buffer for the pellets. Fraction identity and content were verified using western blotting.

Endosome trafficking

Endocytic trafficking was measured using a previously described assay reporting on the recycling of Alexa Fluor 555-conjugated transferrin from human serum (Invitrogen) (Magadan et al., 2006). After a 1 hr incubation in DMEM without FBS containing 2 mg/ml BSA to remove endogenous transferrin, cells grown on coverslips were allowed to take up Alexa Fluor 555-conjugated transferrin (25 µg/ml) at 37 °C for 30 minutes. After transferrin internalization, cells were washed with PBS containing 0.5 % BSA and chased during 0, 5, 15, 30 or 60 min at 37 °C in DMEM containing 2 mg/ml unlabeled

transferrin and 100 µM deferoxamine mesylate. At the end of each treatment time, cells were washed with PBS containing 0.5 % BSA and processed for microscopic examination after fixation in PFA and nucleus staining with 4',6-diamidino-2-phenylindole (DAPI). All images were acquired on a Zeiss AxioImager.z1 equipped with an ApoTome module for structured illumination microscopy using the Axiovision software (Zeiss). Fluorescence intensity was normalized to the number of cell nuclei in each image with a minimum of 100 cells analyzed per condition.

Intracellular proteolysis

General protease activity was assessed by visualization of the intracellular degradation of fluorogenic substrate DQ green BSA (Invitrogen), resulting in dequenching and the release of fluorescence. Cells grown on coverslips were incubated with 10 µg/mL of DQ-BSA for 1 hr at 37 °C, fixed, and nuclei were stained with DAPI. All images were acquired on a Zeiss AxioImager.z1 equipped with an ApoTome module for structured illumination microscopy using the Axiovision software (Zeiss). Fluorescence intensity was normalized to the number of cell nuclei in each image with a minimum of 100 cells analyzed per condition.

Total cathepsin activity was determined from the cleavage of fluorogenic substrates (Calbiochem): Bz-Arg-Gly-Phe-Phe-Pro-4MβNA (Substrate I) for cathepsin D; Z-Phe-Arg-7-amido-4-methylcoumarin (Substrate II) for cathepsins B, S, K and L; and Z-RR-AMC (Substrate III) for cathepsin B. Cells were washed twice with ice-cold PBS and total cell extracts were obtained by osmotic shock (100 mM sodium acetate in distilled water at pH 5.5 in order to maintain enzymatic activity). To assess acidic protease activity, samples were diluted in acetate buffer pH 5.5 (100 mM sodium acetate, 2 mM EDTA, and 2 mM DTT), and fluorescence release was continuously measured at λ_{Ex}= 355 nm and λ_{Em}= 460 nm at 30 °C on a VICTOR X Multilabel plate reader (PerkinElmer).

Evaluation of acidic vesicle content

Acidic vesicles were labeled using the acidotropic dye acridine orange based on its pH-dependent spectral shift (green fluorescence in the cytosol and red fluorescence in acidic vesicles) (Huang et al., 2009). Cells washed in HBSS were incubated for 15 minutes with 1 µg/ml of acridine orange solution (Sigma). After 2 washes in HBSS, fluorescence at λ_{Em} 535 and 615 nm (λ_{Ex} = 485 nm) was measured on a VICTOR X Multilabel Plate Reader (PerkinElmer). The 615/535 fluorescence ratio was used to quantify the size of the acidic vesicular compartment, and data were normalized to control conditions for each independent experiment.

LAMP1 staining was used to probe for lysosome abundance/surface and distribution (distance relative to cell nuclei) using the particle measurement tool of the ImageJ software 1.46r (Hissa et al., 2012). The surface area of each LAMP1-stained particle was expressed in µm² from calibrated images. Mean lysosomal distance from nucleus was calculated with the x and y coordinates of each particle with respect to each cell nucleus. Data are expressed in mean distance (µm) for each condition. A minimum of 20 cells were counted per condition.

Intracellular pH measurements

Lysosomal pH was measured after overnight endocytosis by intact cells of 0.5 mg/ml of pH sensitive FITC-dextran (Sigma) prepared in DMEM (Vidal-Donet et al., 2013). FITC-dextran in excess was removed by washes in HBSS, followed by 1 hr incubation in HBSS with the indicated treatments. Calibration was performed with the addition of 10 µM nigericin (Invitrogen) and 20 µM monensin (Sigma) in Hepes-buffered HBSS adjusted to different pH with HCl or NaOH. Images were acquired on an AxioImager.z1 microscope equipped with an ApoTome module for structured illumination microscopy using the Axiovision software with Filter set 38 (all from Zeiss). Fluorescence intensities of 5 to 10 images per condition were transformed in pH values using the calibration curve.

Cytosolic pH was measured using the cell-permeable probe 5,6-carboxy-SNARF-1 acetoxymethyl ester acetate (SNARF-1-AM) following manufacturer's indications. Briefly, cells washed with HBSS were incubated with 7 µM SNARF-1-AM for 30 min at 37 °C. Excess dye was removed by washes in HBSS, and fluorescence emission at 580 and 642 nm (λ_{Ex} = 485 nm) was recorded on a VICTOR X Multilabel plate reader. Calibration was performed with the addition of 2.5 µM nigericin (Invitrogen) in Hepes-buffered HBSS-based solution containing 120 mM KCl adjusted to different pH with HCl or KOH to equilibrate extracellular and intracellular pH. Fluorescence ratio 642/580 was converted to pH values using the calibration curve according to manufacturer's protocol.

Vesicle maturation

To monitor autophagosome maturation, a mRFP-GFP-LC3-encoding plasmid (Plasmid 21074: ptfLC3, Addgene) was used according to (Kimura et al., 2007). Detection takes advantage of the different pH sensitivities of GFP and mRFP in a fusion protein with LC3 and targeted to autophagy vesicles. Briefly, the GFP fluorescent signal is quenched at acidic pH, whereas mRFP is not. Therefore, the LC3 fusion protein localized in immature not acidic autophagosome emits GFP and mRFP fluorescence, whereas it emits only mRFP fluorescence when localized in mature acidic autolysosomes. Images were acquired on an AxioImager.z1 microscope equipped with an ApoTome module for structured illumination microscopy using the Axiovision software (all from Zeiss). For each cell, GFP^+RFP^+, GFP^-RFP^+ and total vesicles were quantified using the particle analysis tool of ImageJ software 1.46r, with a minimum of 40 cells per condition.

Fusion of lysosomes with autophagosomes to form autolysosomes was evaluated by calculation of Pearson co-localization coefficient for LAMP1 and LC3 immunostaining with JACoP (Bolte and Cordelieres, 2006) for ImageJ software 1.46r. A coefficient of 1 corresponds to a perfect co-localization and a decrease in Pearson coefficient was related to a decrease in fusion between autophagosomes and lysosomes.

SUPPLEMENTAL REFERENCES

Bolte, S., and Cordelieres, F.P. (2006). A guided tour into subcellular colocalization analysis in light microscopy. J. Microsc. *224*, 213-232.

Bouzin, C., Saini, M.L., Khaing, K.K., Ambroise, J., Marbaix, E., Gregoire, V., and Bol, V. (2016). Digital pathology: elementary, rapid and reliable automated image analysis. Histopathology *68*, 888-896.

Breul, S.D., Bradley, K.H., Hance, A.J., Schafer, M.P., Berg, R.A., and Crystal, R.G. (1980). Control of collagen production by human diploid lung fibroblasts. J. Biol. Chem. *255*, 5250-5260.

Hissa, B., Duarte, J.G., Kelles, L.F., Santos, F.P., del Puerto, H.L., Gazzinelli-Guimaraes, P.H., de Paula, A.M., Agero, U., Mesquita, O.N., Guatimosim, C. et al. (2012). Membrane cholesterol regulates lysosome-plasma membrane fusion events and modulates Trypanosoma cruzi invasion of host cells. PLoS. Negl. Trop. Dis. *6*, e1583.

Huang, B., Meng, N., Zhao, B., Zhao, J., Zhang, Y., Zhang, S., and Miao, J. (2009). Protective effects of a synthesized butyrolactone derivative against chloroquine-induced autophagic vesicle accumulation and the disturbance of mitochondrial membrane potential and Na+,K+-ATPase activity in vascular endothelial cells. Chem. Res. Toxicol. *22*, 471-475.

Lakhter, A.J., Sahu, R.P., Sun, Y., Kaufmann, W.K., Androphy, E.J., Travers, J.B., and Naidu, S.R. (2013). Chloroquine promotes apoptosis in melanoma cells by inhibiting BH3 domain-mediated PUMA degradation. J. Invest Dermatol. *133*, 2247-2254.

Mizushima, N., and Yoshimori, T. (2007). How to interpret LC3 immunoblotting. Autophagy. *3*, 542-545.